Legionella pneumophila modulates host energy metabolism by ADP-ribosylation of ADP/ATP translocases

Jiaqi Fu[1], Mowei Zhou[2], Marina A. Gritsenko[3], Ernesto S. Nakayasu[3], Lei Song[4]* and Zhao-Qing Luo[1]*

[1]Department of Biological Science, Purdue University, West Lafayette, IN 47907, USA

[2]Environmental and Molecular Sciences Division, Pacific Northwest National Laboratory, Richland, WA 99352, USA

[3]Biological Science Division, Pacific Northwest National Laboratory, Richland, WA 99352, USA

[4]Department of Respiratory Medicine and Center of Infection and Immunity, Key Laboratory of Organ Regeneration and Transplantation of the Ministry of Education, The First Hospital, Jilin University, Changchun, China

*Correspondence: lsong@jlu.edu.cn and luoz@purdue.edu

Abstract

The intracellular pathogen *Legionella pneumophila* delivers more than 330 effectors into host cells by its Dot/Icm secretion system. Those effectors direct the biogenesis of the *Legionella*-containing vacuole (LCV) that permits its intracellular survival and replication. It has long been documented that the LCV is associated with mitochondria and a number of Dot/Icm effectors have been shown to target to this organelle. Yet, the biochemical function and host cell target of most of these effectors remain unknown. Here, we found that the Dot/Icm substrate Ceg3 (Lpg0080) is a mono-ADP-ribosyltransferase that localizes to the mitochondria in host cells where it attacks ADP/ATP translocases by ADP-ribosylation, and blunts their ADP/ATP exchange activity. The modification occurs on the second arginine residue in the -RRRMMM- element, which is conserved among all known ADP/ATP carriers from different organisms. Our results reveal modulation of host energy metabolism as a virulence mechanism for *L. pneumophila*.

Key words: Type IV secretion; mART; ADP-ribosylation; ATP/ADP transport

Introduction

Legionella pneumophila, a Gram-negative intracellular bacterial pathogen, is the causative agent of Legionnaires' disease. This bacterium exists ubiquitously in the environment as a parasite of fresh water amoebae (1). Infection of humans occurs when susceptible individuals inhale aerosol contaminated by bacteria and introduce the pathogen to the lungs where it is phagocytosed by alveolar macrophages. Instead of being digested, engulfed bacteria survive and replicate in macrophages, leading to tissue damage and strong inflammatory responses and the development of disease symptoms (2). The cell biological characteristics of infected amoebae and mammalian cells are highly similar, both are featured by the formation of an endoplasmic reticulum (ER)-like phagosome called the *Legionella*-containing vacuole (LCV), which in the initial phase of infection, bypasses the endocytic pathways of the phagocytes (3). The biogenesis of the LCV requires the Dot/Icm system, which is arguably the most important pathogenic factor of *L. pneumophila* (4). Mutations in any component gene essential for the function of the Dot/Icm transporter result in a complete loss of virulence on all hosts. This multicomponent machine injects more than 330 virulence factors known as effectors into host cells to construct the LCV by manipulating diverse cellular processes, including vesicle trafficking, autophagy, lipid metabolism, and cytoskeleton structure via distinct biochemical activities (5).

A common mechanism utilized by bacterial effectors is to function as enzymes that attack specific host proteins involved in important cellular processes by posttranslational modifications (PTMs) (6), including phosphorylation (7), AMPylation (8), phosphorylcholination (9, 10), ubiquitination (11, 12) and ADP-ribosylation (12, 13). Among these, ADP-ribosylation is one of the first identified PTMs utilized by toxins from bacterial pathogens (14); this modification is catalyzed by ADP-ribosyltransferases (ARTs) that transfer the ADP-ribose moiety from nicotinamide adenine dinucleotide (NAD) to target substrates via an *N*-, *O*-, or *S*- glycosidic linkage (15). Depending on the property of the enzymes, the modification can be the addition of either one (mono) or more (poly) ADP-ribosyl moieties onto the recipient site of the target proteins (16). In addition to virulence factors from bacterial pathogens, ARTs have been identified in

eukaryotic proteins, which regulate such important cellular processes as DNA damage repair, gene expression and aging (17). Differing from ARTs of bacterial origins, which often are mono-ADP-ribosyltransferases (mARTs), many mammalian enzymes are poly (ADP-ribose) polymerases (PARPs) that induce the formation of poly ADP-ribose (PAR) chains on substrate molecules (16).

Bacterial toxin-induced mono-ADP-ribosylation attacks a wide spectrum of host functions to benefit the pathogens. Some of the best studied examples include the inhibition of host protein synthesis by the diphtheria toxin that modifies elongation factor 2 (EF2) (18) and the interference of the host second messenger cAMP production by the cholera toxin, which ADP-ribosylates the Gαs subunit of the adenylate cyclase and locks the enzyme in an active form (19). A number of virulence factors injected into host cells by specialized protein secretion systems also use ADP-ribosylation to modulate host functions. For example, the type III effector ExoS of *Pseudomonas aeruginosa* targets multiple cellular proteins, including Ras, the modification of which leads to the inhibition of ROS production by neutrophils (20). Recently, Xu *et al* found that the T3SS effector SopF from *Salmonella enterica* serovar Typhimurium attacks the ATP6V0C subunit of v-ATPase by ADP-ribosylation, thus blocking the recruitment of ATG16L1 to suppress autophagy (21). ADP-ribosylation of important signaling molecules such as ubiquitin has also been documented. One such example is CteC from *Chromobacterium violaceum*, which specifically modifies ubiquitin on Thr66 with a cryptic mART motif to disrupt host ubiquitin signaling (22).

Modification by mono-ADP-ribosylation has recently emerged as an important arsenal for *L. pneumophila* virulence. The effector Lpg0181 was found to inactivate the glutamate dehydrogenase in host cells using an mART activity (13). Members of the SidE effector family catalyze ubiquitination of multiple host proteins by first activating ubiquitin via ADP-ribosylation on Arg42 with an mART activity (12). The activated ubiquitin (ADPR-Ub) is then utilized by a phosphodiesterase activity embedded in the same proteins to catalyze the transfer of phosphoribosyl ubiquitin to serine residues of substrates (12, 23, 24).

Herein, we show that the *L. pneumophila* effector Ceg3 (Lpg0080) localizes to the mitochondrion where it targets carrier proteins of the ADP/ATP translocase family by ADP-ribosylation, leading to the inhibition of the ADP/ATP exchange in mitochondria. Our results uncover the modulation of energy transport as a virulence mechanism for a bacterial pathogen.

Results

The *L. pneumophila* effector Ceg3 is a putative mART that localizes to the mitochondrion

A number of *L. pneumophila* effectors have been found to use mART activity to modulate host functions ranging from metabolism to ubiquitination (12, 13). To identify additional effectors with potential mART activity, we used the HHpred algorithm (25) to analyze established Dot/Icm substrates (26, 27). These efforts identified Ceg3 (Lpg0080), a 255-residue protein as a putative mART. The key residues in the predicted mART of Ceg3 are identical to those of bacterial toxins or effector proteins, including ExoS of *Pseudomonas aeruginosa* (20), CtxA of *Vibrio cholera* (19), and members of the SidE family of *L. pneumophila* (12). The sequence of the predicted mART in Ceg3 is R_{44}-S_{94}-$E_{141}KE_{143,}$ which resides in its central region (**Fig. 1A**).

Ceg3 was first identified as a Dot/Icm substrate by virtue of being coregulated with known effector genes (28) and was later shown to kill the yeast *Saccharomyces cerevisiae* upon ectopic expression (29). To determine whether the putative mART motif plays a role in its yeast toxicity, we constructed the $Ceg3_{E/A}$ mutant in which both of the predicted catalytic sites E141 and E143 were replaced with alanine. Comparing to wild-type protein that severely inhibited yeast growth, $Ceg3_{E/A}$ has completely lost the toxicity (**Fig. 1B**). These results suggest that the putative mART motif is critical for the activity of Ceg3.

To understand the function of Ceg3, we first determined its cellular localization. Results from pilot experiments indicated that the distribution of Flag-Ceg3 is not

cytosolic, we thus co-stained it with the cytochrome c oxidase subunit 4 isoform 1 (COX4I1) and Calnexin, marker for mitochondrion and the ER, respectively. The staining signals of Flag-Ceg3 overlap extensively with those of COX4I1 but not Calnexin (**Fig. 1C**), suggesting that Ceg3 localizes to the mitochondria. We also included MavC, an *L. pneumophila* effector targeting to the cytoplasm (11), as an additional control, which did not co-localize with COX4I1 (**Fig. 1C**). Similarly, immunogold labelling results using transmission electron microscopy showed that Flag-Ceg3 was associated with the mitochondria (**Fig. 1D**). Thus, Ceg3 likely is targeted to the mitochondria once being injected into host cells.

We further analyzed the subcellular localization of Ceg3 by cell fractionation. Cells transfected to express Flag-Ceg3 or Flag-MavC were mechanically lysed and the mitochondrial fractions were obtained by centrifugation as described (30). Samples from each fraction were separated by SDS-PAGE and analyzed by immunoblotting with antibodies against Flag and resident proteins of the relevant organelles, respectively. Flag-Ceg3 co-fractionated with the subunit α1 of pyruvate dehydrogenase E1 (PDHA1), which is an established mitochondrial marker (31). In agreement with results from immunostaining experiments, Flag-Ceg3 did not co-fractionate with Calnexin and GM130, markers for the ER and the Golgi apparatus, respectively. In contrast, Flag-MavC co-fractionated with the cytosolic protein tubulin (**Fig. 1E**). These results corroborate well with the immunostaining data, further indicating mitochondrial localization of Ceg3.

The association of Ceg3 with mitochondria can be mediated either by binding to mitochondrial proteins or by integrating into its membranes. To distinguish between these two possibilities, we treated mitochondria isolated from cell expressing HA-Ceg3 with a high pH buffer (0.1 M Na_2CO_3, pH 11) and separated integral and peripheral membrane proteins by centrifugation. Two peripheral membrane proteins, cytochrome c (Cyto-C) and the beta subunit of ATP synthase (ATPB) that are associated with inner mitochondrial membranes (32, 33), can be stripped from the mitochondria effectively by the high pH buffer (**Fig. 1F**). In contrast, HA-Ceg3 was only detected in the pellet

fraction together with the mitochondrial import receptor subunit TOM20 homolog (Tom20) and the voltage-dependent anion-selective channel protein 1 (VDAC1), two integral mitochondrial membrane proteins (34, 35). Thus, Ceg3 is not peripherally associated with mitochondrial membranes.

ADP/ATP translocases (ANTs) are the cellular targets of Ceg3

To identify the cellular targets of Ceg3, we first determined its ability to induce ADP-ribosylation of host proteins upon transfection. To this end, we used a pan-ADP-ribose antibody (36) to detect ADP-ribosylated proteins in cell transfected to express Ceg3 or the $Ceg3_{E/A}$ mutant. A band slightly larger than 25 kDa was detected in lysates of cells expressing Ceg3 but not in samples expressing $Ceg3_{E/A}$ (**Fig. 2A, left panel and middle panes**). Probing these samples with antibodies specific for Flag and ADP-ribose simultaneously detected two proteins of distinct sizes in samples expressing Flag-Ceg3, indicating that the protein detected by the ADP-ribose antibody was not self-modified Flag-Ceg3 (**Fig. 2A, right panel**). Thus, Ceg3 may ADP-ribosylate one or more host proteins with a size of approximately 25 kDa.

We also performed immunoprecipitation (IP) with beads coated with the Flag antibody in lysates from cells transfected to express Flag-Ceg3 or Flag-$Ceg3_{E/A}$. Several protein bands, including one that migrated at approximately 25 kDa were detected in samples transfected with Flag-Ceg3 or Flag-$Ceg3_{E/A}$ but not the empty vector (**Fig. 2B, right panel**). Furthermore, when probed with the ADP-ribose antibody, strong signals were detected in samples expressing Flag-Ceg3 but not its mutant with a disrupted mART motif (**Fig. 2B, left panel**). Taken together, these results suggest that Ceg3 interacts with one or more host proteins of approximately 25 kDa.

To identify the substrates modified by Ceg3, we enriched ADP-ribosylated proteins from samples of cells transfected to express this effector by using recombinant Af1521, a protein from *Archaeoglobus fulgidus* that contains a macro domain involved in binding ADP-ribose moieties on modified proteins (37). After enrichment, the potential targets of Ceg3 with a molecular weight slightly higher than 25 kDa were detected by

192 silver staining as well as ADP-ribose immunoblotting only in samples expressing Ceg3
193 (**Fig. 2C**). This protein band detected by silver staining was then excised and analyzed
194 by mass spectrometry. Among the top 10 proteins with the most hits, with the exception
195 of keratin, a common contaminant in mass spectrometric samples, four were assigned
196 as ADP/ATP translocases (ANTs) (**Table S1**). We confirmed ANT proteins as
197 substrates of Ceg3 by transfecting mammalian cells to express GFP-Ceg3 and Flag-
198 ANT1, which is one isoform of ADP/ATP translocases, and examined their interactions
199 by IP. Precipitates obtained by beads coated with the Flag antibody contained GFP-
200 Ceg3 (**Fig. 2D**), indicating the binding between these two proteins. Consistent with
201 these results, fluorescence signals of GFP-Ceg3 colocalize extensively with those of
202 RFP-ANT1 (**Fig. 2E**).
203
204 Human cells express four ADP/ATP translocase isoforms, each was identified in
205 our mass spectrometric analysis (**Table S1**). ANTs are essential for transferring ADP
206 and ATP across the mitochondrial inner membranes (38), which is consistent with our
207 finding that Ceg3 is targeted to this organelle (**Fig. 1C-F**). Collectively, these results
208 indicate that ANTs are the potential targets of Ceg3.
209
210 **Ceg3 ADP-ribosylates ANTs on an arginine residue in a conserved element**
211 To examine whether that Ceg3 targets all ANT isoforms by ADP-ribosylation, we
212 co-expressed Flag-tagged each of the four isoforms (ANT1, ANT2, ANT3 and ANT4)
213 with GFP-Ceg3 or GFP-Ceg3$_{E/A}$ in HEK293T cells and isolated Flag-ANTs proteins from
214 cell lysates by IP. Detection using the ADP-ribose probe revealed that each of the ANTs
215 was modified by Ceg3 but not the mutant Ceg3$_{E/A}$ (**Fig. 3A**). These results demonstrate
216 that Ceg3 modifies these ADP/ATP translocases by ADP-ribosylation.
217
218 We next used ANT1 as the model to determine the site of modification. Mass
219 spectrometric analysis of samples using wild-type ANT1 suggested that the modification
220 likely occurs around Arg237 but the exact site could not be precisely assigned due to
221 the large size of the peptides produced by protease trypsin or Lys-C from this region.
222 We thus replaced Val227 and Arg237 with Lys in order to generate peptides of sizes

more suitable for detection upon Lys-C digestion. The introduction of these mutations did not affect Ceg3-induced modification of ANT1 (**Fig. S1A**). When $ANT1_{V227K/R237K}$ purified from cells co-expressing Ceg3 or $Ceg3_{E/A}$ (**Fig. S1B**) were analyzed by mass spectrometry analysis, a mass shift of 541.06 Da matching to mono-ADP-ribosylation on the peptide -S_{228}YPFDTVRRK$_{237}$- in $ANT1_{V227K/R237K}$ was detected only in samples co-expressing Ceg3. MS/MS spectra showed that the modification mapped to residue Arg236, and the modified peptide produced several fragmented ions with *m/z* of 136.1, 250.1, 348.1 and 428.0 which are adenine, adenosine, adenosine monophosphate (AMP) and adenosine diphosphate (ADP), respectively, all are diagnostic fragments of the ADPR moiety (**Fig. 3B**) (39). We also detected a series of fragments containing the conversion of arginine to ornithine residues (-42 Da), which is also diagnostic tandem mass fragment of ADP-ribosylated arginine residues (40). Thus, Ceg3 modifies ANT1 by mono-ADP-ribosylation on residue Arg236.

The structure of the bovine ADP/ATP carrier (>90% identity to that from humans) (41), reveals that ANTs are consisting of six transmembrane helices and three matrix loops (**Fig. 3C**). In ANT1, the modified site Arg236 resides in the end of the fifth transmembrane region, which is close to the matrix side of the mitochondrion (41). Sequence alignment of the four mammalian ANT isoforms shows that the site modified by Ceg3 mapped to the second Arg residue of the conserved -RRRMMM- element (**Fig. S2**), which has been shown to be important for the transport activity of ANTs (41). We next confirmed the modification site in ANT1 by testing mutants with lysine substitutions in each of several conserved Arg residues (i.e. Arg60, Arg72, Arg138, Arg140, Arg152) that are close to the interface between the transmembrane helices and the matrix loops of ANT1 and each of the three Arg residues (i.e. Arg235, Arg236 and Arg237) in the -R_{235}RRMMM$_{240}$- motif. Only mutations in Arg236 abolished Ceg3-induced ADP-ribosylation (**Fig. 3D**). These results establish that Ceg3 specifically modifies Arg236 in the conserved -R_{235}RRMMM$_{240}$ motif in ANT1.

ADP/ATP carriers are evolutionarily conserved in eukaryotes, which in *S. cerevisiae* are represented by three isoforms, Aac1p, Aac2p and Aac3p. These proteins

have molecular weights similar to those of their mammalian counterparts and each harbors the -RRRMMM- element (42). Given that Ceg3 inhibits the growth of yeast in an mART motif-dependent manner, we determined whether Ceg3 induces ADP-ribosylation of yeast ADP/ATP carrier proteins. Although the expression of His_6-Ceg3 in yeast cells was not detectable with a His_6-specific antibody, ADP-ribosylation of proteins with a molecular weight close to those of ADP/ATP carriers was detected in lysates of yeast cells expressing Ceg3 but not $Ceg3_{E/A}$ (**Fig. 3E**). Thus, yeast ADP/ATP carriers are also targeted by Ceg3 for ADP-ribosylation modification, which likely accounts for its toxicity.

We attempted to establish biochemical reactions to study Ceg3-induced ADP-ribosylation of ANTs by preparing recombinant Ceg3 from *E. coli*. Yet, none of the commonly used tags allowed the production of soluble Ceg3 under various induction conditions (**Fig. S3A**) as well as several truncated mutants of Ceg3 (**Fig. S3B**). The insoluble property of Ceg3 is consistent with the fact that Ceg3 is not a peripheral protein of the mitochondria (**Fig. 1E**).

We then purified Flag-GFP-Ceg3 and Flag-GFP-$Ceg3_{E/A}$ from transfected mammalian cells and tested their ability to modify similarly purified Flag-ANTs by ADP-ribosylation. Although endogenous ANTs in cells expressing Flag-GFP-Ceg3 were modified, incubation of purified Ceg3 and ANT1 with NAD did not lead to detectable modification (**Fig. S4A**). Importantly, when co-expressed in *E. coli*, Ceg3-induced ANT1 modification was detectable, again in a manner that requires the mART motif (**Fig. S4B**). The ability of Ceg3 to modify ANT1 in *E. coli* indicates that this enzyme functions without the need of co-factors from eukaryotic cells.

The ADP/ATP carriers are ADP-ribosylated by Ceg3 in cells infected with *L. pneumophila*

To examine whether the observed modification of ANTs by Ceg3 occurs under physiological conditions, we attempted to detect the modification during *L. pneumophila* infection. It was clearly detectable in samples infected with a strain that lacks the

chromosomal *ceg3* but expresses the gene from a multicopy plasmid (**Fig. 4A**). ANTs modification in infected cells was also detected in cells infected with the wild-type strain harboring the plasmid but not in a mutant defective in the Dot/Icm transporter (**Fig. 4B**). Modification of ANTs was not detected by wild-type strain at 2 h post infection (psi) (**Fig. 4A**), which may be due to the temoporal regulation. We then extended the infection time to 18 h and sampled infected cells at 4-h intervals. Under this experimental condition, ADP-ribosylation of ANTs induced by WT *Legionella* became detectable at 6 h after bacterial uptake and peaked at 10 h. Furthermore, the level of modification decreased at 14 h and was maintained at low level till 18 h (**Fig. 4C**), which corresponds to maximal intracellular replication in this host cell (43). This modification pattern suggest that *L. pneumophila* temporally regulates ANTs by ADP-ribosylation either by differently controlling the expression of Ceg3 at different phases of infection or by injecting enzymes capable of reversing the modification at infection phases beyond 10 h. Taken together, these results indicate that Ceg3 induces ADP-ribosylation of ANTs during *L. pneumophila* infection. The inability to detect modification at 2 h psi may be due to low abundancy of translocated Ceg3 or modified ANTs have not reached the quantity detectable by the method we used.

We also examined the role of Ceg3 in intracellular replication of *L. pneumophila* using the Δ*ceg3* mutant in mouse bone marrow-derived macrophages and the protozoan host *Dictyostelium discoideum*. Akin to most Dot/Icm substrates that are dispensable for intracellular replication in laboratory infection models, the Δ*ceg3* mutant grew at rates indistinguishable to those of the wild-type strain (**Fig. S5**), suggesting that the absence of Ceg3 does not detectably affect the intracellular replication of *L. pneumophila* in commonly used laboratory hosts.

Ceg3 inhibits ANTs-mediated ADP/ATP exchange in mitochondria

The main role of mitochondrion is ATP production and regulation of metabolism flux, and the production of ATP entirely depends on the integrity of mitochondrial membrane potential (MMP) (44). We thus examined whether Ceg3-induced ADP-ribosylation of ANTs compromises MMP. HEK293T cells transfected to express Ceg3 or

its mutants for 24 h were loaded with the JC-10 dye, which, in healthy mitochondria, forms aggregates that emits red fluorescence signals but diffuses out of mitochondria with damaged MMP and exhibits green fluorescence signals (45). As expected, treatment with the ionophore carbonyl cyanide m-chlorophenyl hydrazine (CCCP) that damages the MMP by uncoupling the proton gradient, rendered the cells to emit green fluorescence signals (**Fig. 5A**) (46). The expression of Ceg3 but not $Ceg3_{E/A}$ caused a slight decrease in MMP. Thus, the impact of Ceg3 on mitochondrial membrane integrity, if any, is moderate.

ATP is transported across the inner mitochondrial membrane by ANTs via exchange with ADP at a 1:1 stoichiometry (47), we next examined the impact of Ceg3-induced modification on this by adding 2 mM ADP into mitochondria isolated from HEK293T cells transfected to express Ceg3 or its mutants and determined the amounts of released ATP (**Fig. 5B**). Expression of Ceg3 but not $Ceg3_{E/A}$ in HEK293T cells caused a decrease in ADP/ATP exchange (**Fig. 5C**). Moreover, such inhibition also occurred in mitochondria isolated from cells infected with *L. pneumophila* strains capable of inducing detectable ANT ADP-ribosylation (**Fig. 5D**). Together, these results indicate that ADP-ribosylation of ANTs by Ceg3 blocks ADP/ATP exchange by mitochondria (**Fig. 5E**).

ANTs modified by ADP-ribosylation maintain their role in mitophagy induction

A recent study showed that ANT1 is critical for the induction of mitophagy (48), which is a branch of autophagy involved in the degradation of damaged mitochondria (49). We thus examined whether Ceg3-induced ADP-ribosylation of ANTs affects their roles in mitophagy. After testing a few cell lines, we found that COS-1 cells undergo robust mitophagy upon being treated with the protonophores CCCP, which caused a clear loss of two mitochondrial proteins, PDHA1 and ATPB (**Fig. S6A**). To ensure that Ceg3 is expressed in a high percentage of cells in the samples, we prepared lentiviral particles that direct Ceg3 expression. Transduction of COS-1 cells with our lentiviral particles led to mART-dependent ADP-ribosylation of endogenous ANTs (**Fig. S6B**). Under our experimental conditions in which cells were uniformly transduced and the

expression of Ceg3 is readily detectable, the levels of PDHA1 were similar among all samples (**Fig. S6C**), suggesting that Ceg3 did not induce mitophagy. We also tested the effect of Ceg3 on CCCP-induced mitophagy. While treatment with this protonophore did lead to a drastic decrease in PDHA1, such decrease did not detectably change between samples expressing Ceg3 or $Ceg3_{E/A}$ (**Fig. S6C**). Thus, Ceg3 does not suppress or augment CCCP-induced mitophagy.

Discussion

In addition to powering most cellular activities by ATP production, mitochondria are involved in diverse functions such as cell death, immunity and metabolism regulation (50). As a result, this organelle is a common target for infectious agents that actively manipulate host cellular processes for their survival and replication (51). For example, the *Vibrio cholera* T3SS effector VopE inhibits the activity of Miro1 and Miro2, two mitochondrial GTPases, by functioning as a GTPase-activating protein (GAP), thus suppressing host innate immune responses (52). The effector ECH0825 from *Ehrlichia chaffeensis* upregulates the mitochondrial manganese superoxide dismutase to prevent ROS-induced cellular damage and mitochondria-mediated apoptosis (53).

Earlier cell biological studies suggest that mitochondrion plays important roles in the intracellular life cycle of *L. pneumophila*. The association of the LCV with mitochondria was documented in morphological analysis of its infection cycle within several years after the bacterium was recognized as a pathogen. As least 30% of LCVs were surrounded by mitochondria within 15 min of phagocytosis, which increases to approximately 65% when the infection proceeds to one hour (54). This observation was validated by more recent studies, which reveal that such association requires the Dot/Icm transporter essential for *L. pneumophila* virulence (55).

A number of Dot/Icm effectors have been demonstrated to modulate the function of mitochondria. Among these, LegS2, a homologue of the eukaryotic enzyme sphingosine-1-phosphate lyse, contributes to autophagy inhibition by disrupting lipid metabolism in mitochondria (56, 57). MitF appears to modulate mitochondrial dynamics

by provoking a Warburg-like effect to benefit intracellular bacterial replication (58). Our results here demonstrate that Ceg3 specifically localizes to mitochondria where it modifies members of the ADP/ATP translocase by mono-ADP-ribosylation, leading to inhibition of ADP/ATP exchange in mitochondria.

ADP-ribosylation of ANTs induced by Ceg3 is readily detectable in yeast and mammalian cells that are ectopically expressing the effector (**Fig. 2A and Fig. 3E**). Due to technical barriers to obtain soluble recombinant Ceg3, we were unable to establish a reaction with purified proteins to show Ceg3-induced ADP-ribosylation of ANTs. The fact that such modification occurs when Ceg3 and ANT1 were co-expressed in *E. coli* indicates that no host cell co-factor is required for its activity (**Fig. S4B**). The detection of ANT modification in cells infected with wild-type *L. pneumophila* validates the translocases as its *bona fide* substrates.

The ADP-ribosylation site on ANT1 induced by Ceg3 is Arg236, which is the second Arg residue in the -RRRMMM- element conserved in not only all four ADP/ATP translocases of mammalian origin, but also all known ADP/ATP carriers from different organisms (59). The three arginine residues in the -RRRMMM- motif are essential for the transport function of the yeast ADP/ATP carrier Aac2 (60, 61). Mutations in each of these three arginine residues in the bovine ADP/ATP carrier abolish its transport activity, so does a mutation in Arg246 (equivalent to Arg236 in mammalian ANT1) of the mitochondrial carrier from *Thermothelomyces thermophile* (41, 62). These observations are consistent with our results that ADP-ribosylation of one of these three sites ablates its ADP/ATP transport activity (**Fig. 5C-D**). Moreover, our finding that Ceg3 does not interfere with mitophagy is in line with a previous study showing that the ADP/ATP translocase-associated mitophagy is independent of its nucleotide translocase activity (48).

Structure of the bovine ADP/ATP carrier shows that Arg236 of ANT1 is localized in the end of the fifth transmembrane helix, which is in close proximity to the mitochondrial matrix (41). In the Aac2 carrier from yeast, the -RRRMMM- element

appears to be in the mitochondrial matrix (42). Although the positioning of the -RRRMMM- element revealed by these two structural analyses slightly differs, both studies conclude that the second arginine is implicated in ADP binding via its positively charged side chain that mediates electrostatic interactions with the negatively charged phosphate moieties in ADP (41, 42). At neutral pH, ADP-ribose harbors two negatively charged phosphate moieties, which can cause a notable change in the charge property of the side chain of this arginine residue (63). Thus, Ceg3-mediated ADP-ribosylation on ANTs likely affects the electrostatic interactions with ADP. In addition, the bulky ADPR moiety on ANTs may cause steric interference for the interaction, both of which can contribute to the inhibition of their ADP/ATP exchange ability.

Interestingly, the Dot/Icm effector LncP, which is homologous to mitochondrial carrier proteins, has been suggested to carry out unidirectional ATP transport across membranes reconsitituted in liposomes (64). Although the possibility that Ceg3 coordinates its activity with LncP in *L. pneumophila* infected cells needs further investigation, it is conceivable that the bacterium can gain better control of ATP transport in the mitochondria if it uses one set of effectors to inhibit the endogenous carriers and another set to substitute this function. The number of Dot/Icm effectors that function to modulate mitochondrial activity seems large. An earlier study found that Lpg1625 and Lpg0898 are targeting to this organelle (65). Lpg2444 was recently shown to protect the integrity of mitochondria by making it resistant to MMP damage caused by protonophores such as CCCP. This protein also interacts with ADP/ATP translocase 2, but the biological significance of such interactions is elusive (66). Future study aiming at biochemical analysis of these proteins and their cellular targets in host cells will shed light onto the roles of mitochondria in *L. pneumophila* virulence as well as the mechanism of how the diverse activities of this organelle are regulated.

Methods

Media, bacteria strains, plasmid construction and cell lines

Escherichia coli strains were grown on LB agar plates or in LB broth. When necessary, antibiotics were added to media at the following concentrations: ampicillin, 100 μg/mL; kanamycin, 30 μg/mL. *L. pneumophila* strains used in this study were derivatives of the Philadelphia 1 strain Lp02 (67). Lp03 is an isogenic *dotA*$^-$ mutant (68). All strains were grown and maintained on CYE plates or in ACES-buffered yeast extract (AYE) broth as previously described (67). For *L. pneumophila,* antibiotics were used at: kanamycin, 20 μg/mL, streptomycin, 100 μg/mL. When needed, thymidine was added at a final concentration of 100 μg/mL. Other methods are available in Supplementary Information.

Plasmid construction and cell lines

The oligonuecleotides, plasmids and bacterial strains used in this study were listed in Table S2. The Δ*ceg3* in-frame deletion strain was constructed by a two-step allelic exchange strategy as described (69). For complementation experiments, genes were inserted into pZLQ-Flag, a derivative of pZLQ (70) that was modified to carry a Flag tag. For ectopic expression of proteins in mammalian cells, genes were inserted into pEGFPC1 (Clontech), the 4xFlag CMV vector (71) or pAPH, a derivative of pVR1012 (72) suitable for expressing proteins with an amino HA tag and a carboxyl Flag tag. To co-express Ceg3 and ANT1 in *E. coli*, *ceg3* and *ANT1* were inserted into pZLQ-Flag and pGEX-6p-1 (GE Healthcare), respectively. The integrity of all constructs was verified by sequencing analysis. HEK293T, HeLa or COS-1 cells purchased from ATCC were cultured in Dulbecco's modified minimal Eagle's medium (DMEM) supplemented with 10% Fetal Bovine Serum (FBS). Bone marrow-derived macrophages were prepared from 6- to 10-week-old female A/J mice (Jackson Lab) with L-cell supernatant-conditioned medium as described previously (73). All mammalian cell lines were regularly checked for potential mycoplasma contamination by the universal mycoplasma detection kit from ATCC (Cat# 30-1012K).

Yeast toxicity assays

All yeast strains used in this study were derived from W303 (10); yeast was grown at 30°C in YPD medium or in appropriate amino acid dropout synthetic media supplemented with 2% of glucose or galactose as the sole carbon source. Yeast transformation was performed as previously described (74). Inducible protein toxicity of Ceg3 was assessed by the galactose-inducible promoter on pYES1NTA (Invitrogen). Briefly, plasmids harboring Ceg3 or its mutant derived from pYES1NTA were transformed into yeast strain W303. Yeast grown in liquid selective medium in the presence of glucose was serially diluted five-fold and 5 μL of each dilution was spotted onto selective plates containing glucose or galactose. Plates were incubated at 30°C for 3 days before image acquisition.

Carbonate treatment of mitochondria

Mitochondria were isolated from cultured cells using a mitochondria isolation kit (Thermo Fisher, cat# 89874) according to the manufacturer's instructions. Isolated mitochondria were resuspended in a high pH carbonate buffer (0.1 M Na_2CO_3, pH 11) on ice for 30 min with occasional agitation. Samples were centrifuged at 15,000 *g* for 20 min at 4°C. Integral membrane proteins were collected in pellet fraction, while peripheral membrane proteins and soluble proteins were harvested in supernatant fraction. Both fractions were resolved by SDS-PAGE and analyzed by immunoblotting.

Transfection, immunoprecipitation, infection

Plasmids were transfected into mammalian cells by using Lipofectamine 3000 (Invitrogen, cat# L3000150). After 24 h transfection, cells were collected and lysed with the TBS buffer (150 mM NaCl, 50 mM Tris-HCl, pH 7.5) with 1% Triton X-100. When needed, immunoprecipitation was performed with lysates of transfected cells by using beads coated with the Flag antibody (Sigma, cat# F2426) at 4°C overnight. Beads were washed with pre-cold lysis buffer for 3 times. All samples were resolved by SDS-PAGE and followed by immunoblotting analysis with the specific antibodies. For ADP-ribosylated proteins enrichment by Af1521 pulldown, Affigel beads (BioRad) were coated with recombinant His-Af1521 proteins with protocols supplied by the manufacturer and then were incubated with lysates of HEK293T cells transfected to

express Ceg3 or $Ceg3_{E/A}$ overnight at 4°C. Affigel beads were washed 3 times and bound proteins were treated with SDS sample buffer. Proteins resolved by SDS-PAGE were visualized by silver staining and immunoblotting.

For all *L. pneumophila* infection experiments, *L. pneumophila* strains were grown in AYE broth to the post-exponential phase judged by optical density (OD_{600nm}= 3.2-4.0) as well as increase in motility. Complementation strains were induced with 0.2 mM isopropyl β-D-1-thiogalactopyranoside (IPTG) for 4 h at 37°C before infection. To determine the modification of ANTs and ADP/ATP exchange rates in mitochondria during bacterial infection, HEK293T cells transfected to express FCγRII receptor (12) for 24 h were infected with opsonized bacteria at a multiplicity of infection (MOI) of 100. 2 h after infection, mitochondria were isolated from cells for further experiments. For assays of *L. pneumophila* growth within, approximately $4x10^5$ bone marrow-derived macrophages or *D. discoideum* seeded into 24-well plates 1 day before infection were infected with relevant *L. pneumophila* at an MOI of 0.05. 2 hours after adding the bacteria, we synchronized the infection by washing the monolayers three times with PBS buffer. Infected macrophages or *D. discoideum* were incubated at 37°C in the presence of 5% CO_2 or at 25°C, respectively. At each time point, cells were lysed with 0.02% saponin, dilutions of the lysate were plated onto bacteriological media, and CFU were determined from triplicate wells of each strain.

Protein purification

For His-Af1521 protein production, 10 mL overnight *E. coli* cultures were transferred to 400 mL LB medium in the presence of 100 μg/mL ampicillin and grown to OD_{600nm} of 0.6-0.8. Then the cultures were incubated at 18 °C for 16-18h after the addition of IPTG at a final concentration of 0.2 mM. Bacterial cells were harvested at 12,000*g* by spinning and lysed by sonication. The soluble lysates were cleared by spinning at 12,000*g* twice at 4°C for 20 min. His-tagged proteins were purified with Ni^{2+}-NTA beads (QIAGEN) and were eluted with 300 mM imidazole in PBS buffer. Purified proteins were dialyzed in buffer containing PBS, 5% glycerol and 1 mM DTT overnight.

Antibodies and Immunoblotting

For immunoblotting, samples resolved by SDS-PAGE were transferred onto 0.2 μm nitrocellulose membranes (Bio-Rad, cat# 1620112). Membranes were blocked with 5% non-fat milk, and then incubated with the appropriate primary antibodies: anti-HA (Sigma, cat# H3663), 1:5000; anti-Flag (Sigma, cat# F1804), 1: 5000; anti-ICDH (75), 1:10,000; anti-tubulin (DSHB, E7) 1:10,000; anti-PDHA1 (Proteintech, cat# 18068-1-AP), 1:5000; anti-ATPB (Proteintech, cat# 17247-1-AP), 1:2000; anti-TOM20 (Proteintech, cat# 11802-1-AP), 1:5000; anti-VDAC1 (Proteintech, cat# 55259-1-AP), 1:2000; anti-Cyto c (Santa Cruz, cat# sc-13560), 1:1000; anti-Calnexin (Proteintech, cat# 10427-2-AP), 1:2000; anti-GM130 (BD Biosciences, cat# 610822), 1:2500; anti-ADPR (Sigma, cat# MABE1016), 1:1000. Membranes were then incubated with an appropriate IRDye infrared secondary antibody and scanned by using an Odyssey infrared imaging system (Li-Cor's Biosciences).

Immunostaining

HEK293T Cells were seeded at $5x10^4$ per well on glass coverslips in 24-well plates 1 day before transfection. Cells were transfected to express corresponding proteins for 24 h, and then fixed by 4% formaldehyde solution for 20 min at room temperature. Fixed cells were permeabilized by 0.2% Triton X-100 solution for 5 min, and blocked with 4% goat serum for 30 min at 37 °C. COX4I1 was stained with the COX4I1 specific antibody (Cell signaling, cat# 4850) at a dilution of 1:500, Calnexin was stained with the Calnexin specific antibody (Proteintech, cat# 10427-2-AP) at a dilution of 1:500, Flag was stained with the Flag specific antibody (Sigma, cat# F1804) at a dilution of 1:50. Incubation with primary antibodies was performed overnight at 4°C, and then cells were stained with secondary antibodies conjugated to Alexa Flour 594 or Alexa Flour 488 (Thermo Fisher Scientific) at a dilution of 1:500 for 1 h at room temperature. After staining for nucleus with Hoechst, samples were analyzed by using an IX-81 Olympus fluorescence microscope and images were pseudocoloured with the IPLab software.

Lentiviral transduction

To produce lentivirus for transduction expression of Ceg3 in COS-1 cells, Ceg3 was inserted into pCDH-CMV-MCS-EF1a-RFP (System Biosciences cat# CD512B-1), which was transfected together with pMD2.G (Addgene plasmid #12259) and psPAX2 (Addgene plasmid #12260) vector (76) into HEK293T cells grown to about 70% confluence. Supernatant was collected after 48 h and then filtered with a 0.45 μm syringe filter. The titer of the produced lentivirus was determined by using qPCR Lentivirus Titer Kit (abm, cat# LV900). For lentiviral transduction, approximately $1x10^5$ COS-1 cells seeded into 24-well plates 1 day before transduction were transduced with lentiviral particles at an MOI of 10. Cells incubated for 2 days at 37°C with 5% CO_2 were collected for immunoblotting.

Detection of mitochondrial membrane potential (MMP)

The MMP was measured using a mitochondria membrane potential kit from Sigma (Cat# MAK159) as previously described (77). Briefly, approximately $5x10^4$ HEK293T cells were seeded in opaque 96-well plates with clear bottom 1 day before transfection. After 18 h of transient expression, 50 μL JC-10 Dye loading solution was added to each sample well and incubated at 5% CO_2, 37°C for 1 h, then 50 μL of assay buffer B was added. The intensity of red fluorescence (λ_{ex}=540/λ_{em}=590 nm) and green fluorescence (λ_{ex}=490/λ_{em}=525 nm) was monitored by a BioTek reader (Synergy 2, BioTek). The ratio of red/green fluorescence intensity was used to determine MMP. Samples treated by 20 μM CCCP for 1 h was applied as a positive control of MMP loss.

ADP/ATP exchange rates determination

Mitochondria isolated from one 10-cm plate of HEK293T cells transfected to express the proteins of interest or infected with relevant *L. pneumophila* strains were washed three times and resuspended in a reaction buffer (10 mM HEPES (pH 7.4), 250 mM sucrose and 10 mM KCl). The ADP/ATP exchange process was initiated by the addition of ADP at a final concentration of 2 mM. After 5 min incubation, the amount of ATP transported from mitochondria was determined using an ATP measurment kit (Invitrogen, cat# A22066). Luminescence of samples was detected by a BioTek reader (Synergy 2, BioTek). For each experiment, a standard curve was generated with serially

diluted ATP and was used to calculate the concentration of ATP in samples to determine ADP/ATP exchange rates.

Immunogold labeling

HEK293T cells transiently expressing Flag-Ceg3 were washed with PBS briefly and fixed overnight with 4% formaldehyde and 0.5% glutaraldehyde in 0.1 M phosphate buffer (PB), pH 7.4 at 4°C. Cells were then washed with 0.1 M PB three times and then incubated in 0.1 M glycine solution (pH 2.2) for 20 min to quench the free aldehyde groups. The cell pellet was rinsed in 0.1 M PB buffer, and then dehydrated in an ascending ethanol series and infiltrated with LR white resin. Samples were embedded in gelatin capsules and polymerized. Polymerized samples were sectioned on a ultramicrotome and 60-70 nm thick sections were collected onto 200 mesh nickel grids. Grids were blocked with PBS containing 1% bovine serum albumin (BSA) (PBS-BSA buffer) for 30 min at 37°C and then incubated with the anti-FLAG M2 monoclonal antibody (Sigma, cat# F1804) at a 1:50 dilution in the PBS-BSA buffer overnight at 4°C. The grids were rinsed with the same buffer five times and then were incubated with anti-mouse IgG conjugated with 10 nm gold particles (Sigma, cat# G7652) at a 1:10 dilution in 1% BSA-PBS for 1 hour. Grids were then washed with PBS and distilled water to remove unbound gold conjugate. The labeled samples were then post-stained with uranyl acetate and washed by distilled water prior to being examined by a Tecnai T12 (WSLR S046) transmission electron microscopy.

LC-MS/MS analysis

Protein bands were digested in-gel with trypsin/Lys-C for protein identification or Lys-C for ADP-ribosylation modification site identification as previously described (78). Digested peptides were injected onto a Waters NanoAcquity liquid chromatography (LC) system, coupled to Thermo Orbitrap Eclipse or Lumos. The LC has a dual pump configuration. Samples were desalted on a 4 cm reversed-phase trapping column (in-house packed, 150 µm i.d. 5 µm Jupiter C18 particle from Phenomenex) at 5 µL/min for 10 min. The analytical separation was on a 70 cm reversed-phase column (in-house packed, 75 µm i.d. 3 µm Jupiter C18 particle from Phenomenex) at 0.3 µL/min over 2 h.

Mobile phases are 0.1% formic acid in water for A, and 0.1% formic acid in acetonitrile for B. The gradient started at 1% B, and ramped to 8%-12%-30%-45%-95% B at 2-20-75-97-100 min, respectively.

MS source was set to 2.2 kV for electrospray, 250°C for capillary inlet and RF lens at 30%. Acquisition method is data-dependent peptide mode with cycle time of 3 s. Isolation window was 1.6 *m/z*. Alternating higher-energy collisional dissociation (HCD) and electron transfer dissociation (ETD) were applied to the same precursor. HCD had stepped energy of 20, 30, 40%. ETD reaction time follows the calibrated parameters, with supplemental HCD of 20%. Resolution setting was 60k for MS1 and 30k for MS2. Normalized AGC target was 250% for MS1, 100% for HCD, and 200% for ETD. Injection time control was set to auto.

For protein identification, the raw data were processed with the software Mascot (version 2.3.02, Matrix Science) against *Homo sapiens* database (Uniprot, UP000005640). Mascot was set to search with the following parameters: peptide tolerance at 0.05 Da, MS/MS tolerance at 0.2 Da, carbamidomethyl (C) as a fixed modification, oxidation (M) as a variable modification, and maximum of two missed cleavage. The false-discovery rates (FDR) were controlled at <1%. To identify the ADP-ribosylation modification sites, data were analyzed using Byonic v3.11 (ProteinMetrics). Protein FASTA contained the target protein and common contaminations (trypsin, keratin, etc as provided in Byonic). Semi-specific and two max missed cleavages were allowed. Mass error tolerance was 7 ppm for precursor and 10 ppm for fragments. Dynamic modifications (provided in Byonic) include carbamidomethyl (+57.02 Da), oxidation (+15.99 Da), phosphorylation (+79.97 Da), and ADP-ribosylation (+541.06 Da). Custom modifications included phosphoribosylation (+212.01 Da), ADP (+409.02 Da), AMP (+329.20 Da), and ribosylation (+132.04 Da). Identified peptides were then examined manually for spectral quality. High confidence peptides with target modifications were further examined manually in Xcalibur QualBrowser.

Data quantitation and statistical analyses

653 Student's *t*-test was used to compare the mean levels between two groups each
654 with at least three independent samples. All western blot results shown are one
655 representative from three independent experiments.
656

Acknowledgements

The authors thank Dr. Shaohua Wang for plasmids, Dr. Victor Roman for making pZLQ-Flag, Mr. Karl Weitz and Mr. Ronald Moore for assistance in mass spectrometry analysis. We thank Dr Christopher J. Gilpin, Dr. Robert Seiler and Dr. Laurie Mueller for their support in TEM analysis which was performed at the Purdue Electron Microscopy Facility. This work in part was supported by National Institutes of Health grant R01AI127465 (ZQL) and by Jilin Science and Technology Agency grant 20200403117SF (LS). Mass spectrometry analysis was performed in the Environmental Molecular Sciences Laboratory, a U.S. Department of Energy (DOE) national scientific user facility at Pacific Northwest National Laboratory (PNNL) in Richland, WA. Battelle operates PNNL for the DOE under contract DE-AC05-76RLO01830.

Author contributions JF, SL and ZQL conceived the projects, JF performed the experiments. MZ, MG and ESN performed the mass spectrometric analysis of modification site identification. JF, MZ, ESN, SL and ZQL analyzed data. JF drafted the first version of the manuscript, JF and ZQL revised the manuscript with input from all authors.

References

1. Richards AM, Von Dwingelo JE, Price CT, & Abu Kwaik Y (2013) Cellular microbiology and molecular ecology of Legionella-amoeba interaction. *Virulence* 4:307-314.
2. Newton HJ, Ang DK, van Driel IR, & Hartland EL (2010) Molecular pathogenesis of infections caused by Legionella pneumophila. *Clin Microbiol Rev* 23:274-298.
3. Isberg RR, O'Connor TJ, & Heidtman M (2009) The Legionella pneumophila replication vacuole: making a cosy niche inside host cells. *Nat Rev Microbiol* 7:13-24.
4. Hubber A & Roy CR (2010) Modulation of host cell function by Legionella pneumophila type IV effectors. *Annu Rev Cell Dev Biol* 26:261-283.
5. Qiu J & Luo ZQ (2017) Legionella and Coxiella effectors: strength in diversity and activity. *Nat Rev Microbiol* 15:591-605.
6. Salomon D & Orth K (2013) What pathogens have taught us about posttranslational modifications. *Cell Host Microbe* 14:269-279.
7. Lee PC & Machner MP (2018) The Legionella Effector Kinase LegK7 Hijacks the Host Hippo Pathway to Promote Infection. *Cell Host Microbe* 24:429-438 e426.
8. Muller MP*, et al.* (2010) The Legionella effector protein DrrA AMPylates the membrane traffic regulator Rab1b. *Science* 329:946-949.
9. Mukherjee S*, et al.* (2011) Modulation of Rab GTPase function by a protein phosphocholine transferase. *Nature* 477:103-106.
10. Tan Y, Arnold RJ, & Luo ZQ (2011) Legionella pneumophila regulates the small GTPase Rab1 activity by reversible phosphorylcholination. *Proc Natl Acad Sci U S A* 108:21212-21217.
11. Gan N, Nakayasu ES, Hollenbeck PJ, & Luo ZQ (2019) Legionella pneumophila inhibits immune signalling via MavC-mediated transglutaminase-induced ubiquitination of UBE2N. *Nat Microbiol* 4:134-143.
12. Qiu J*, et al.* (2016) Ubiquitination independent of E1 and E2 enzymes by bacterial effectors. *Nature* 533:120-124.
13. Black MH*, et al.* (2021) A Legionella effector ADP-ribosyltransferase inactivates glutamate dehydrogenase. *J Biol Chem*:100301.
14. Aravind L, Zhang D, de Souza RF, Anand S, & Iyer LM (2015) The natural history of ADP-ribosyltransferases and the ADP-ribosylation system. *Curr Top Microbiol Immunol* 384:3-32.
15. Cohen MS & Chang P (2018) Insights into the biogenesis, function, and regulation of ADP-ribosylation. *Nat Chem Biol* 14:236-243.
16. Hottiger MO, Hassa PO, Luscher B, Schuler H, & Koch-Nolte F (2010) Toward a unified nomenclature for mammalian ADP-ribosyltransferases. *Trends Biochem Sci* 35:208-219.
17. Palazzo L, Mikoc A, & Ahel I (2017) ADP-ribosylation: new facets of an ancient modification. *FEBS J* 284:2932-2946.
18. Honjo T, Nishizuka Y, & Hayaishi O (1968) Diphtheria toxin-dependent adenosine diphosphate ribosylation of aminoacyl transferase II and inhibition of protein synthesis. *J Biol Chem* 243:3553-3555.

19. Cassel D & Pfeuffer T (1978) Mechanism of cholera toxin action: covalent modification of the guanyl nucleotide-binding protein of the adenylate cyclase system. *Proc Natl Acad Sci U S A* 75:2669-2673.
20. Vareechon C, Zmina SE, Karmakar M, Pearlman E, & Rietsch A (2017) Pseudomonas aeruginosa Effector ExoS Inhibits ROS Production in Human Neutrophils. *Cell Host Microbe* 21:611-618 e615.
21. Xu Y*, et al.* (2019) A Bacterial Effector Reveals the V-ATPase-ATG16L1 Axis that Initiates Xenophagy. *Cell* 178:552-566 e520.
22. Yan F*, et al.* (2020) Threonine ADP-Ribosylation of Ubiquitin by a Bacterial Effector Family Blocks Host Ubiquitination. *Mol Cell* 78:641-652 e649.
23. Bhogaraju S*, et al.* (2016) Phosphoribosylation of Ubiquitin Promotes Serine Ubiquitination and Impairs Conventional Ubiquitination. *Cell* 167:1636-1649 e1613.
24. Kotewicz KM*, et al.* (2017) A Single Legionella Effector Catalyzes a Multistep Ubiquitination Pathway to Rearrange Tubular Endoplasmic Reticulum for Replication. *Cell Host Microbe* 21:169-181.
25. Soding J, Biegert A, & Lupas AN (2005) The HHpred interactive server for protein homology detection and structure prediction. *Nucleic Acids Res* 33:W244-248.
26. Zhu W*, et al.* (2011) Comprehensive identification of protein substrates of the Dot/Icm type IV transporter of Legionella pneumophila. *PLoS One* 6:e17638.
27. Burstein D*, et al.* (2016) Genomic analysis of 38 Legionella species identifies large and diverse effector repertoires. *Nat Genet* 48:167-175.
28. Zusman T*, et al.* (2007) The response regulator PmrA is a major regulator of the icm/dot type IV secretion system in Legionella pneumophila and Coxiella burnetii. *Mol Microbiol* 63:1508-1523.
29. Urbanus ML*, et al.* (2016) Diverse mechanisms of metaeffector activity in an intracellular bacterial pathogen, Legionella pneumophila. *Mol Syst Biol* 12:893.
30. Chen W*, et al.* (2009) Abcb10 physically interacts with mitoferrin-1 (Slc25a37) to enhance its stability and function in the erythroid mitochondria. *Proc Natl Acad Sci U S A* 106:16263-16268.
31. Borglum AD, Flint T, Hansen LL, & Kruse TA (1997) Refined localization of the pyruvate dehydrogenase E1 alpha gene (PDHA1) by linkage analysis. *Hum Genet* 99:80-82.
32. Walker JE & Dickson VK (2006) The peripheral stalk of the mitochondrial ATP synthase. *Biochim Biophys Acta* 1757:286-296.
33. Garrido C*, et al.* (2006) Mechanisms of cytochrome c release from mitochondria. *Cell Death Differ* 13:1423-1433.
34. Burri L*, et al.* (2006) Integral membrane proteins in the mitochondrial outer membrane of Saccharomyces cerevisiae. *FEBS J* 273:1507-1515.
35. Hiller S*, et al.* (2008) Solution structure of the integral human membrane protein VDAC-1 in detergent micelles. *Science* 321:1206-1210.
36. Shin D*, et al.* (2020) Regulation of Phosphoribosyl-Linked Serine Ubiquitination by Deubiquitinases DupA and DupB. *Mol Cell* 77:164-179 e166.

37. Allen MD, Buckle AM, Cordell SC, Lowe J, & Bycroft M (2003) The crystal structure of AF1521 a protein from Archaeoglobus fulgidus with homology to the non-histone domain of macroH2A. *J Mol Biol* 330:503-511.
38. Klingenberg M (2008) The ADP and ATP transport in mitochondria and its carrier. *Biochim Biophys Acta* 1778:1978-2021.
39. Rosenthal F, Nanni P, Barkow-Oesterreicher S, & Hottiger MO (2015) Optimization of LTQ-Orbitrap Mass Spectrometer Parameters for the Identification of ADP-Ribosylation Sites. *J Proteome Res* 14:4072-4079.
40. Gehrig PM*, et al.* (2021) Gas-Phase Fragmentation of ADP-Ribosylated Peptides: Arginine-Specific Side-Chain Losses and Their Implication in Database Searches. *J Am Soc Mass Spectrom* 32:157-168.
41. Pebay-Peyroula E*, et al.* (2003) Structure of mitochondrial ADP/ATP carrier in complex with carboxyatractyloside. *Nature* 426:39-44.
42. Ruprecht JJ*, et al.* (2014) Structures of yeast mitochondrial ADP/ATP carriers support a domain-based alternating-access transport mechanism. *Proc Natl Acad Sci U S A* 111:E426-434.
43. Derre I & Isberg RR (2004) Legionella pneumophila replication vacuole formation involves rapid recruitment of proteins of the early secretory system. *Infect Immun* 72:3048-3053.
44. Zorova LD*, et al.* (2018) Mitochondrial membrane potential. *Anal Biochem* 552:50-59.
45. Reers M*, et al.* (1995) Mitochondrial membrane potential monitored by JC-1 dye. *Methods Enzymol* 260:406-417.
46. Georgakopoulos ND, Wells G, & Campanella M (2017) The pharmacological regulation of cellular mitophagy. *Nat Chem Biol* 13:136-146.
47. Pfaff E, Klingenberg M, & Heldt HW (1965) Unspecific permeation and specific exchange of adenine nucleotides in liver mitochondria. *Biochim Biophys Acta* 104:312-315.
48. Hoshino A*, et al.* (2019) The ADP/ATP translocase drives mitophagy independent of nucleotide exchange. *Nature* 575:375-379.
49. Youle RJ & Narendra DP (2011) Mechanisms of mitophagy. *Nat Rev Mol Cell Biol* 12:9-14.
50. McBride HM, Neuspiel M, & Wasiak S (2006) Mitochondria: more than just a powerhouse. *Curr Biol* 16:R551-560.
51. Lobet E, Letesson JJ, & Arnould T (2015) Mitochondria: a target for bacteria. *Biochem Pharmacol* 94:173-185.
52. Suzuki M, Danilchanka O, & Mekalanos JJ (2014) Vibrio cholerae T3SS effector VopE modulates mitochondrial dynamics and innate immune signaling by targeting Miro GTPases. *Cell Host Microbe* 16:581-591.
53. Liu H, Bao W, Lin M, Niu H, & Rikihisa Y (2012) Ehrlichia type IV secretion effector ECH0825 is translocated to mitochondria and curbs ROS and apoptosis by upregulating host MnSOD. *Cell Microbiol* 14:1037-1050.
54. Horwitz MA (1983) Formation of a novel phagosome by the Legionnaires' disease bacterium (Legionella pneumophila) in human monocytes. *J Exp Med* 158:1319-1331.

55. Tilney LG, Harb OS, Connelly PS, Robinson CG, & Roy CR (2001) How the parasitic bacterium Legionella pneumophila modifies its phagosome and transforms it into rough ER: implications for conversion of plasma membrane to the ER membrane. *J Cell Sci* 114:4637-4650.
56. Degtyar E, Zusman T, Ehrlich M, & Segal G (2009) A Legionella effector acquired from protozoa is involved in sphingolipids metabolism and is targeted to the host cell mitochondria. *Cell Microbiol* 11:1219-1235.
57. Rolando M*, et al.* (2016) Legionella pneumophila S1P-lyase targets host sphingolipid metabolism and restrains autophagy. *Proc Natl Acad Sci U S A* 113:1901-1906.
58. Escoll P*, et al.* (2017) Legionella pneumophila Modulates Mitochondrial Dynamics to Trigger Metabolic Repurposing of Infected Macrophages. *Cell Host Microbe* 22:302-316 e307.
59. Korver-Keularts IM*, et al.* (2015) Two Novel Mutations in the SLC25A4 Gene in a Patient with Mitochondrial Myopathy. *JIMD Rep* 22:39-45.
60. Muller V, Basset G, Nelson DR, & Klingenberg M (1996) Probing the role of positive residues in the ADP/ATP carrier from yeast. The effect of six arginine mutations of oxidative phosphorylation and AAC expression. *Biochemistry* 35:16132-16143.
61. Nelson DR, Lawson JE, Klingenberg M, & Douglas MG (1993) Site-directed mutagenesis of the yeast mitochondrial ADP/ATP translocator. Six arginines and one lysine are essential. *J Mol Biol* 230:1159-1170.
62. Ruprecht JJ*, et al.* (2019) The Molecular Mechanism of Transport by the Mitochondrial ADP/ATP Carrier. *Cell* 176:435-447 e415.
63. Laing S, Unger M, Koch-Nolte F, & Haag F (2011) ADP-ribosylation of arginine. *Amino Acids* 41:257-269.
64. Dolezal P*, et al.* (2012) Legionella pneumophila secretes a mitochondrial carrier protein during infection. *PLoS Pathog* 8:e1002459.
65. Zhu W, Hammad LA, Hsu F, Mao Y, & Luo ZQ (2013) Induction of caspase 3 activation by multiple Legionella pneumophila Dot/Icm substrates. *Cell Microbiol* 15:1783-1795.
66. Noack J*, et al.* (2020) Dynamic proteomics profiling of Legionella pneumophila infection unveils modulation of the host mitochondrial stress response pathway.
67. Berger KH & Isberg RR (1993) Two distinct defects in intracellular growth complemented by a single genetic locus in Legionella pneumophila. *Mol Microbiol* 7:7-19.
68. Berger KH, Merriam JJ, & Isberg RR (1994) Altered intracellular targeting properties associated with mutations in the Legionella pneumophila dotA gene. *Mol Microbiol* 14:809-822.
69. Dumenil G & Isberg RR (2001) The Legionella pneumophila IcmR protein exhibits chaperone activity for IcmQ by preventing its participation in high-molecular-weight complexes. *Mol Microbiol* 40:1113-1127.
70. Luo ZQ & Farrand SK (1999) Signal-dependent DNA binding and functional domains of the quorum-sensing activator TraR as identified by repressor activity. *Proc Natl Acad Sci U S A* 96:9009-9014.

71. Li G, Liu H, Luo ZQ, & Qiu J (2021) Modulation of phagosome phosphoinositide dynamics by a Legionella phosphoinositide 3-kinase. *EMBO Rep*:e51163.
72. Wang SH*, et al.* (2018) Divergent Pathogenic Properties of Circulating Coxsackievirus A6 Associated with Emerging Hand, Foot, and Mouth Disease. *J Virol* 92.
73. Conover GM, Derre I, Vogel JP, & Isberg RR (2003) The Legionella pneumophila LidA protein: a translocated substrate of the Dot/Icm system associated with maintenance of bacterial integrity. *Mol Microbiol* 48:305-321.
74. Gietz RD, Schiestl RH, Willems AR, & Woods RA (1995) Studies on the transformation of intact yeast cells by the LiAc/SS-DNA/PEG procedure. *Yeast* 11:355-360.
75. Xu L*, et al.* (2010) Inhibition of host vacuolar H+-ATPase activity by a Legionella pneumophila effector. *PLoS Pathog* 6:e1000822.
76. Salmon P & Trono D (2007) Production and titration of lentiviral vectors. *Curr Protoc Hum Genet* Chapter 12:Unit 12 10.
77. Wang M*, et al.* (2019) Long noncoding RNA LINC00336 inhibits ferroptosis in lung cancer by functioning as a competing endogenous RNA. *Cell Death Differ* 26:2329-2343.
78. Shevchenko A, Tomas H, Havlis J, Olsen JV, & Mann M (2006) In-gel digestion for mass spectrometric characterization of proteins and proteomes. *Nat Protoc* 1:2856-2860.

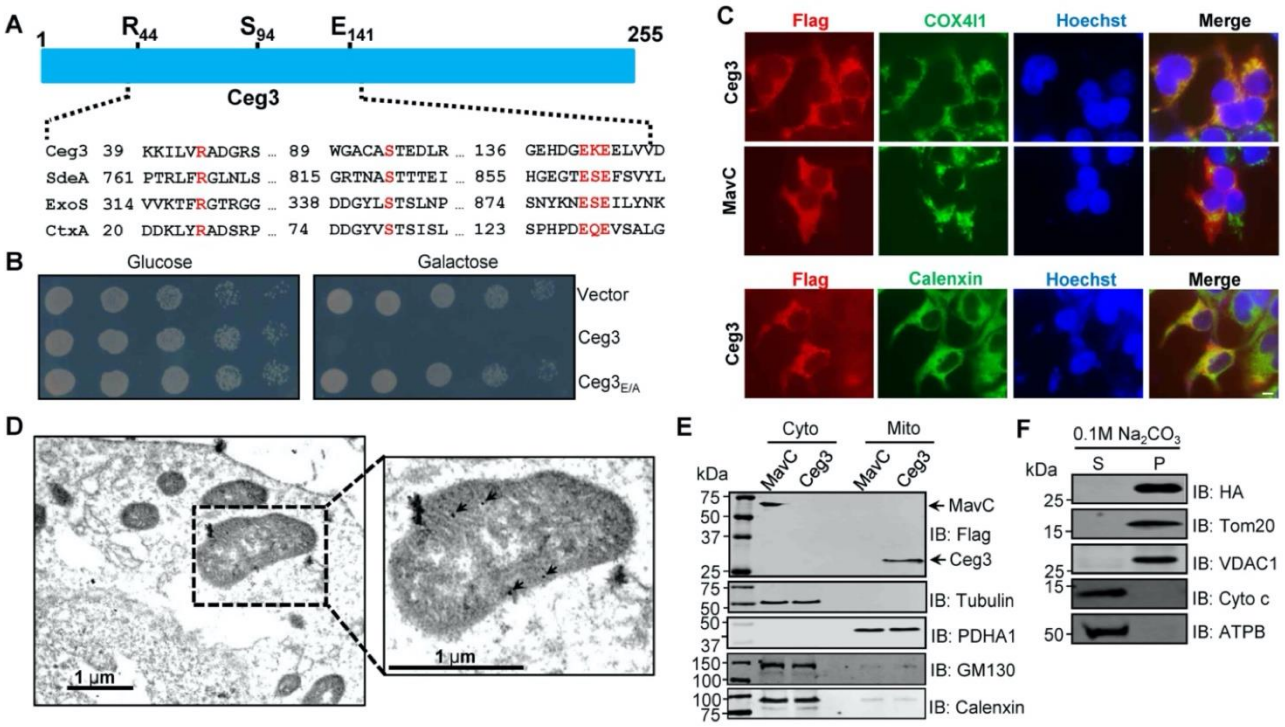

875

876 **Fig. 1 Ceg3 is a mitochondria-associated effector that inhibits yeast growth by a**
877 **putative mART activity**

878 **A**. Sequence alignment of the central region of Ceg3 with three bacterial proteins of
879 mART activity. The strictly conserved residues essential for catalysis are in red. SdeA,
880 ExoS, and CtxA are from *L. pneumophila*, *P. aeruginosa*, and *V. cholerae*, respectively.
881 **B**. The predicted mART motif is critical for Ceg3-mediated yeast toxicity. Serially diluted
882 yeast cells expressing Ceg3 or $Ceg3_{E/A}$ from a galactose-inducible promotor were
883 spotted on the indicated media for 3 days before image acquisition. Similar results were
884 obtained in at least three independent experiments.
885 **C**. Ceg3 co-localizes with the mitochondrial protein COX4I1. HEK293T cells were
886 transfected with plasmids that direct the expression of Flag-Ceg3 or Flag-MavC for 18
887 hours. Fixed samples were immunostained with antibodies specific for Flag (red), the
888 mitochondrial marker COX4I1 or the ER marker Calnexin (green). Images were
889 acquired with an Olympus IX-81 fluorescence microscope. Bar, 5 μm.
890 **D**. Flag-Ceg3 localized to the mitochondria detected by Immunogold labeling. HEK293T
891 cells expressing Flag-Ceg3 were fixed, stained with a mouse anti-Flag antibody and an
892 anti-mouse IgG conjugated with 10 nm gold particles sequentially. Images were

893 acquired with a Tecnai T12 electron microscopy. Area highlighted by rectangles
894 (dashed line) on the left panel is magnified in the right panels. Gold particles were
895 indicated by white arrows. Bar, 1 μm.
896 **E**. Ceg3 fractionated with mitochondria. The cytosol and mitochondrial fractions of
897 HEK293T cells transfected to express Flag-Ceg3 or Flag-MavC were probed with
898 antibodies specific for the indicated proteins.
899 **F**. Ceg3 is an integral mitochondrial membrane protein. Mitochondria isolated from
900 HEK293T cells expressing HA-Ceg3 were subjected to extraction with 0.1 M Na_2CO_3
901 (pH 11) for 30 min. Relevant proteins in soluble (S) and pellet (P) fractions separated by
902 centrifugation were probed by immunoblotting with the indicated antibodies.
903
904

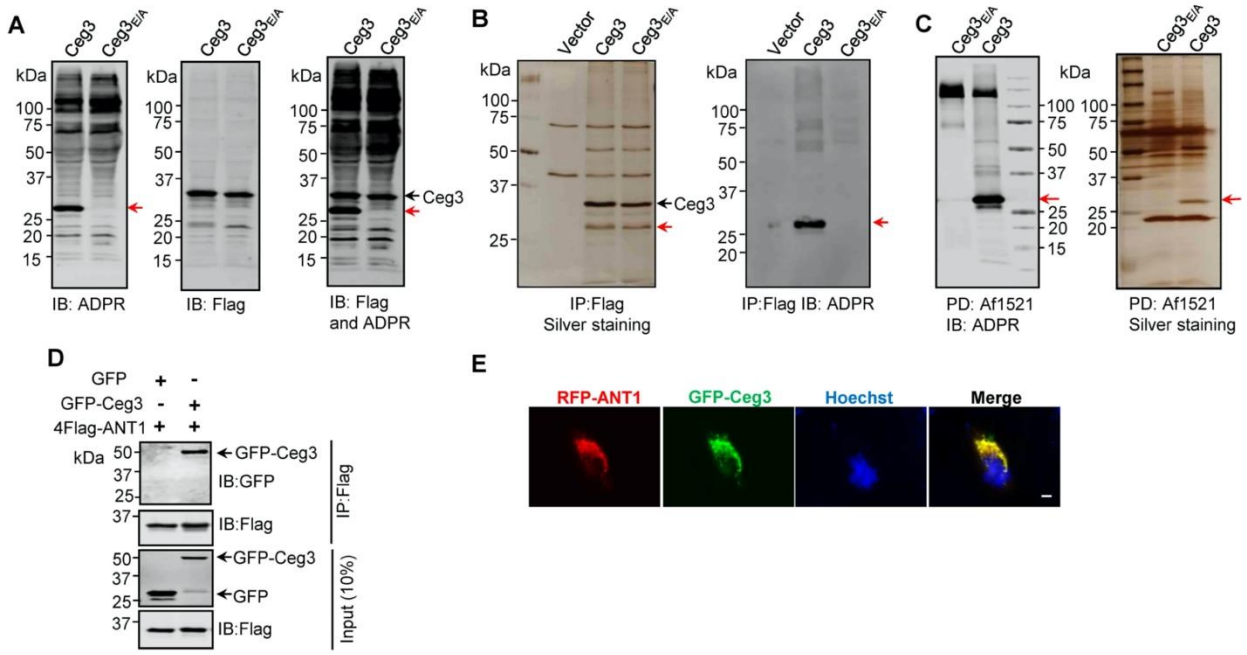

905

906 **Fig. 2 Identification of the cellular targets of Ceg3**

907 **A**. Detection of modified proteins by the ADPR-specific antibody. Lysates of HEK293T
908 cells expressing 4xFlag-Ceg3 or 4xFlag-Ceg3$_{E/A}$ were probed with antibodies specific
909 for ADPR-modification (left), the Flag tag (middle) or both (right). Note that the band
910 indicated by a red arrow in samples expressing Ceg3 detected by the ADPR antibody
911 represents its potential targets.

912 **B**. Substrate probing by immunoprecipitation. Lysates of HEK293T cells transfected to
913 express 4xFlag-Ceg3 or 4xFlag-Ceg3$_{E/A}$ were subjected to immunoprecipitation with
914 beads coated with the Flag antibody and the products resolved by SDS-PAGE were
915 detected by silver staining (left) or probed with the ADPR-specific antibody (right). Note
916 the presence of a band in samples expressing Ceg3 but not Ceg3$_{E/A}$ when detected with
917 the ADPR antibody (red arrows).

918 **C**. Enrichment of ADP-ribosylated proteins by Af1521 from cells transfected to express
919 Ceg3. Lysates of HEK293T cells expressing 4xFlag-Ceg3 or 4xFlag-Ceg3$_{E/A}$ were
920 incubated with beads coated with recombinant Af1521 and the pulldown products
921 resolved by SDS-PAGE were detected by immunoblotting with the ADP-ribose antibody
922 (left) or by silver staining (right) (red arrows).

D. Interactions between ANT1 and Ceg3. Lysates of HEK293T cells co-transfected to express 4xFlag-ANT1 and GFP-Ceg3 (or GFP) were subjected to immunoprecipitation with beads coated with the Flag antibody and bound proteins resolved by SDS-PAGE were detected with Flag and GFP antibodies, respectively. The expression of 4xFlag-ANT1, GFP-Ceg3 and GFP were similarly probed in total cell lysates as input.

E. Colocalization of Ceg3 and ANT1. HeLa cells transfected to express GFP-Ceg3 and RFP-ANT1 were fixed and analyzed. Images were acquired using an Olympus IX-81 fluorescence microscope. Bar, 5 μm.

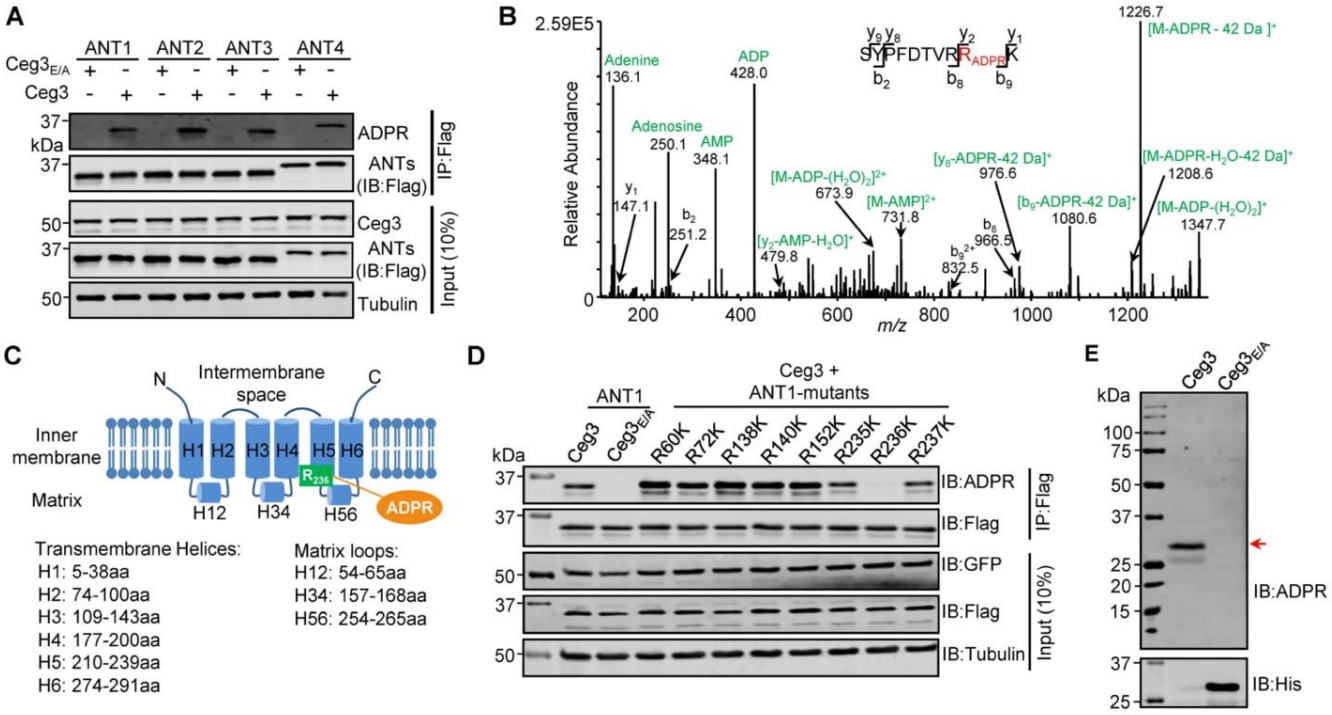

Fig. 3 Determination of the modification sites on ADP/ATP translocases induced by Ceg3

A. Ceg3 attacks all four ANT isoforms by ADP-ribosylation. Flag-tagged ANTs isolated from lysates of cells co-expressing GFP-Ceg3 or GFP-Ceg3$_{E/A}$ by immunoprecipitation were probed with antibodies specific for ADPR and Flag (top). The expression of relevant proteins was probed in total cell lysates with antibodies specific for GFP (Ceg3), Flag (ANTs) and Tubulin (bottom), respectively.

B. Mass spectrometric analysis of ADP-ribosylated 4xFlag-ANT1$_{V227K/R237K}$. Mono-ADP-ribosylation modification was detected in the peptide -S$_{228}$YPFDTVRRK$_{237}$-. Tandem mass (MS/MS) spectrum shows the fragmentation pattern of the modified peptide, with many ADP-ribosylation-specific marker ions and neutral loss fragments highlighted in green.

C. The schematic topology of ANT1 based on the structure of the bovine ADP/ATP carrier (PDB: 1OKC). Note the positioning of Arg236 at the end of helix 5.

D. Mutation of R236 but not neighboring arginine residues in ANT1 abolished Ceg3-induced modification. In each case, Flag-ANT1 or its mutants isolated from HEK293T cells co-expressing GFP-Ceg3 or GFP-Ceg3E/A were probed for ADPR modification (top) or for protein levels in IP products. The expression of Ceg3 and ANT1 or their mutants were probed in total lysates (input). Tubulin was detected as a loading control.

E. Ceg3 induces ADP-ribosylation modification of yeast ADP/ATP carriers. Lysates of yeast cells expressing His_6-Ceg3 or His_6-$Ceg3_{E/A}$ driven by a galactose-inducible promotor were detected for ADPR modification (top) (red arrow) or for the expression of Ceg3 (bottom). Note that the expression of wild-type Ceg3 was not detectable despite the presence of strong modification signals.

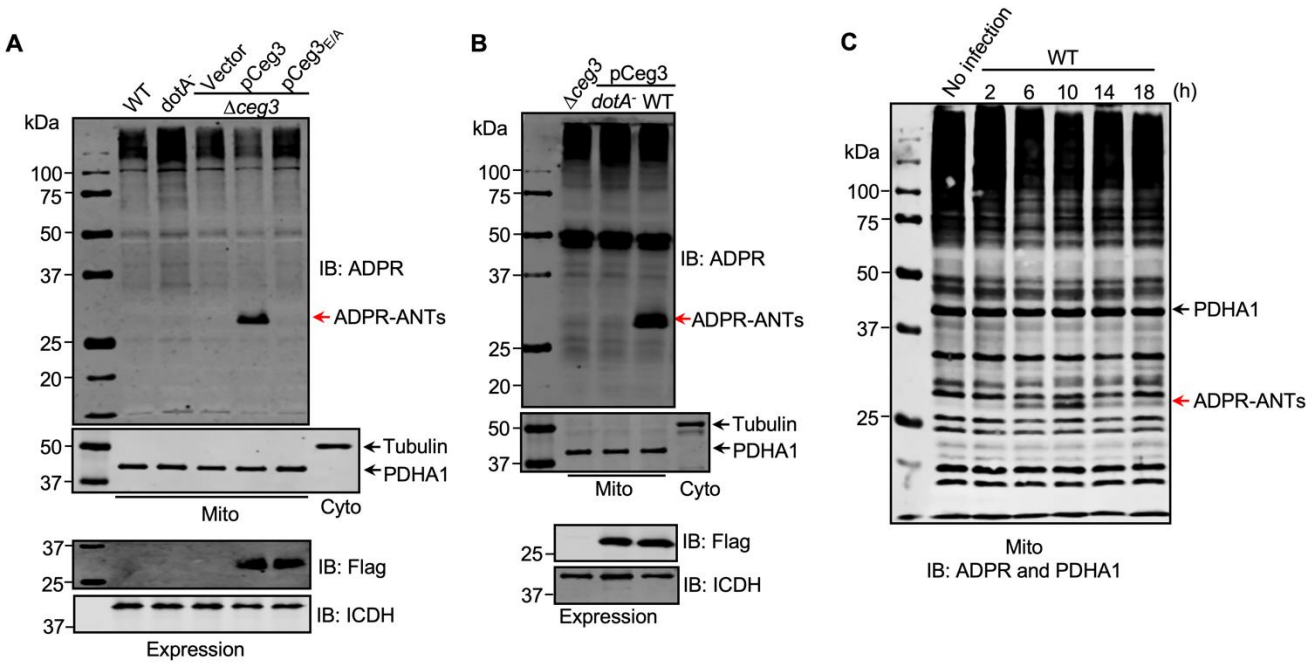

Fig. 4 ADP-ribosylation of ADP/ATP translocases by Ceg3 occurs in cells infected with *L. pneumophila*

A. An intact mART motif in Ceg3 is required for its modification of ADP/ATP translocases during *L. pneumophila* infection. Bacteria of the indicated *L. pneumophila* strains were opsonized prior to infecting HEK293T cells transfected to express the FcγII receptor at an MOI of 100 for 2 h. Samples of the mitochondrial fraction were probed for ADPR after SDS-PAGE (top). PDHA1 and tubulin were probed as controls to monitor the success of cell fractionation. One cytosolic fraction sample was included as an additional control (middle). The expression of Flag-Ceg3 in bacteria was analyzed with the Flag antibody, the metabolic enzyme isocitrate dehydrogenase (ICDH) was probed as a loading control (bottom).

B. A functional Dot/Icm system is required for Ceg3-induced ADP-ribosylation of ADP/ATP translocases in infected cells. HEK293T cells expressing the FcγII receptor were infected with opsonized bacteria expressing Flag-Ceg3 at an MOI of 100 for 2 h. Isolated mitochondrial proteins resolved by SDS-PAGE were probed for ADPR modification (top). The quality of cell fractionation was determined by probing for PDHA1 and tubulin (middle), respectively. The expression of Ceg3 in bacteria was detected with the Flag antibody, and ICDH was probed as a loading control (bottom).

977 **C**. ADP-ribosylation of ADP/ATP translocases is detectably induced by wild-type *L.*
978 *pneumophila* at 6 h post-infection. HEK293T cells expressing the FcγII receptor were
979 infected with opsonized bacteria for the indicated periods of time at an MOI of 30.
980 Mitochondrial proteins were analyzed by anti-ADPR and anti-PDHA1 Western blot.
981

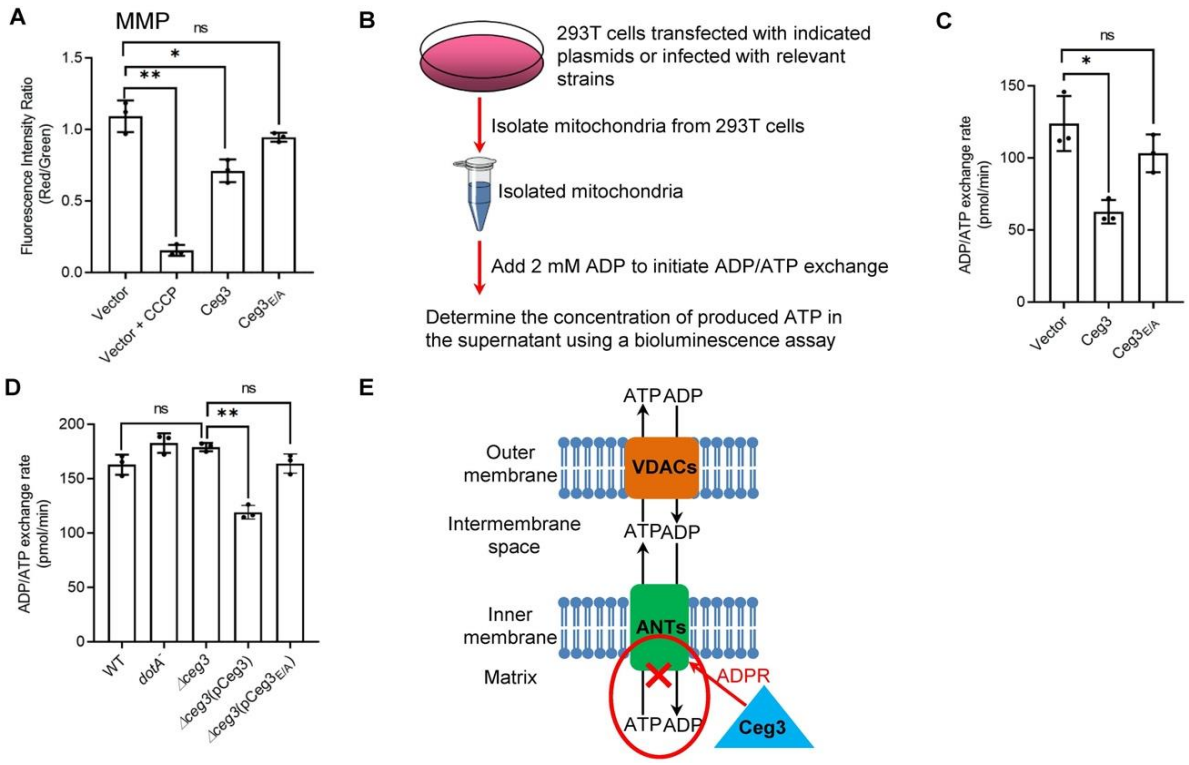

982

983 **Fig. 5 Ceg3 inhibits ADP/ATP exchange in mitochondria**

984 **A**. Ceg3 interferes with the mitochondrial membrane potential (MMP). HEK293T cells
985 transfected to express Ceg3 or its inactive mutant $Ceg3_{E/A}$ were used to determine MMP
986 by the JC-10 dye. Samples treated with 20 μM CCCP for 1 h were included as a
987 positive control for loss of MMP integrity. Quantitation shown was from three
988 independent experiments done in triplicate. Error bars: standard error of the mean
989 (SEM). Statistical analysis was determined by two-tailed *t*-test. ns, not significant; *,
990 $p<0.05$; **, $p<0.01$.

991 **B**. The workflow for measuring ADP/ATP exchange rates.

992 **C**. Ceg3 interferes with the ADP/ATP exchange by mitochondria. Mitochondria isolated
993 from HEK293T cells expressing the indicated proteins were suspended in a reaction
994 buffer containing 10 mM HEPES (pH 7.4), 250 mM sucrose and 10 mM KCl. 2 mM ADP
995 was added to initiate the ADP/ATP exchange process. After 5 min incubation, the
996 concentrations of ATP transported from mitochondria were determined to calculate the
997 ADP/ATP exchange rates. Quantitation shown was from three independent

experiments. Error bars: standard error of the mean (SEM). Statistical analysis was determined by two-tailed *t*-test. ns, not significant; *, $p<0.05$.

D. Ceg3 perturbs ADP/ATP exchange in cells infected with *L. pneumophila*. Opsonized bacteria of the indicated *L. pneumophila* strains were used to infect HEK293T cells expressing the FcγII receptor at an MOI of 100 for 2 h. Mitochondria isolated from the infected cells were used to determine ADP/ATP exchange rates. Results shown were from three independent experiments. Error bars: standard error of the mean (SEM). Statistical analysis was determined by two-tailed *t*-test. ns, not significant; *, $p<0.05$; **, $p<0.01$.

E. A diagram depicting the inhibition of mitochondrial ADP/ATP exchange by Ceg3. Ceg3-induced modification of ANTs by ADPR in the inner membrane blocks the ADP/ATP transport activity of the translocases.

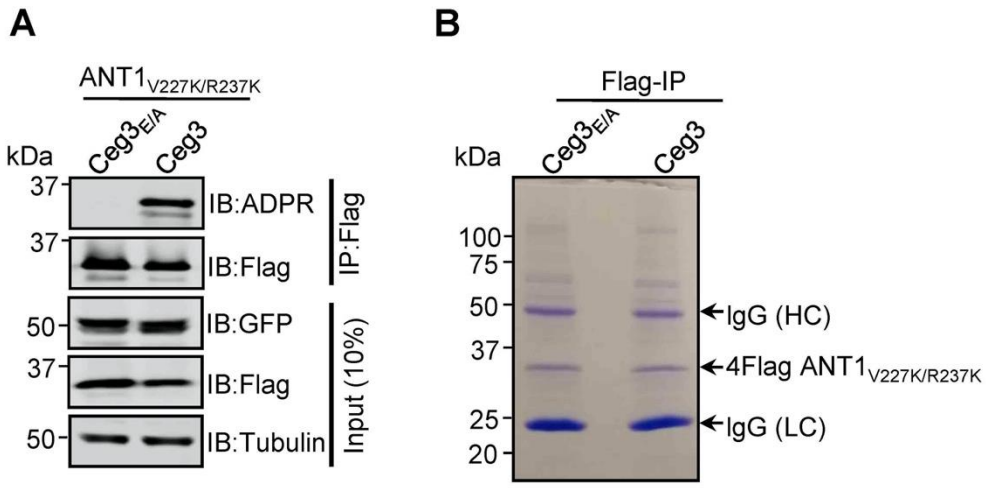

Fig. S1 Lys substitutions of V227 and R237 in ANT1 do not affect Ceg3-induced ADP-ribosylation

A. Ceg3-induced ADPR modification of $ANT1_{V227K/R237K}$. Lysates of HEK293T cells co-transfected to express 4Flag-$ANT1_{V227K/R237K}$ and GFP-Ceg3 or GFP-$Ceg3_{E/A}$ were subjected to immunoprecipitation with Flag beads and the products were detected for ADPR modification or for protein levels. The expression of $ANT1_{V227K/R237K}$ and GFP-Ceg3 was also detected in total cell lysates.

B. Isolation of ADP-ribosylated $ANT1_{V227K/R237K}$ for mass spectrometric analysis. Lysates of HEK293T cells co-expressing 4Flag-$ANT1_{V227K/R237K}$ and GFP-Ceg3 or GFP-$Ceg3_{E/A}$ were immunoprecipitated with Flag beads, and products resolved by SDS-PAGE were detected by Coomassie staining. IgG (HC) and IgG (LC) indicate IgG heavy and light chains.

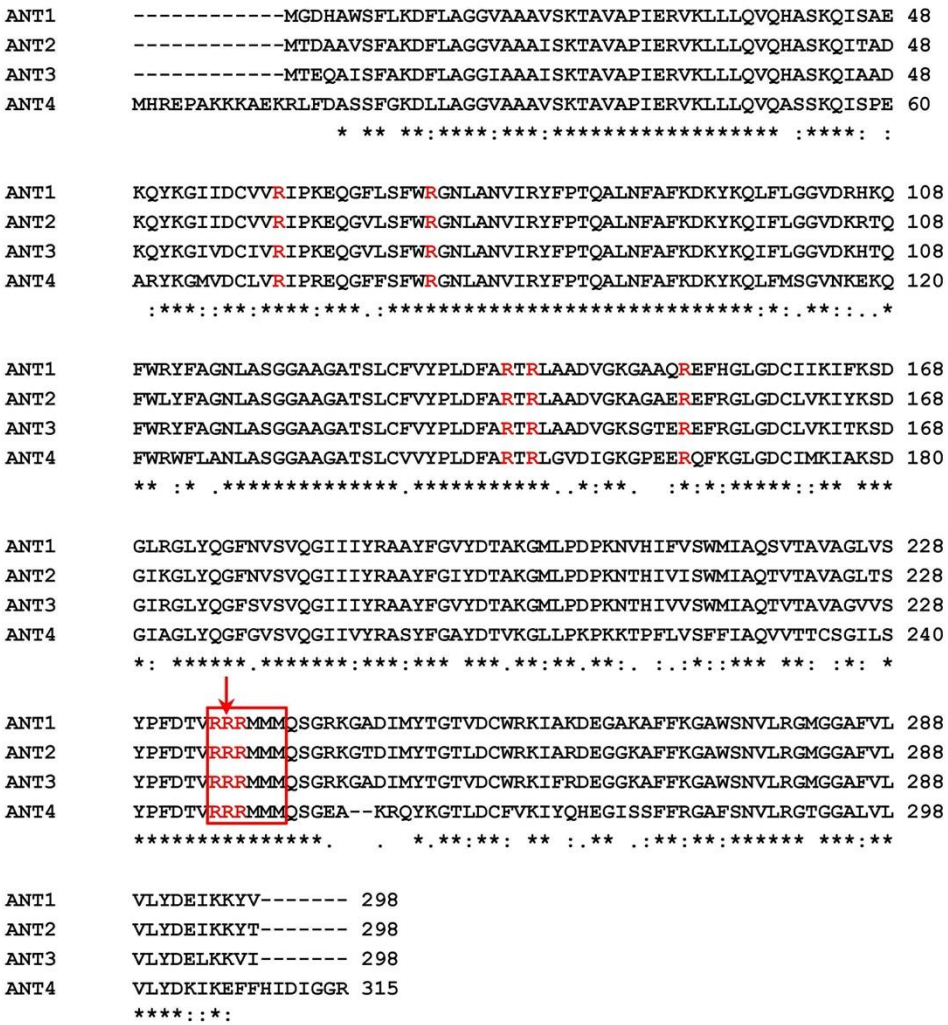

Fig. S2 Sequence alignment of the four human ADP/ATP isoforms. The alignment was generated with the Clustal Omega software. The conserved Arg sites used for mutational analysis were colored in red. The modified sites of ADP-ribosylation mediated by Ceg3 were indicated by a red arrow.

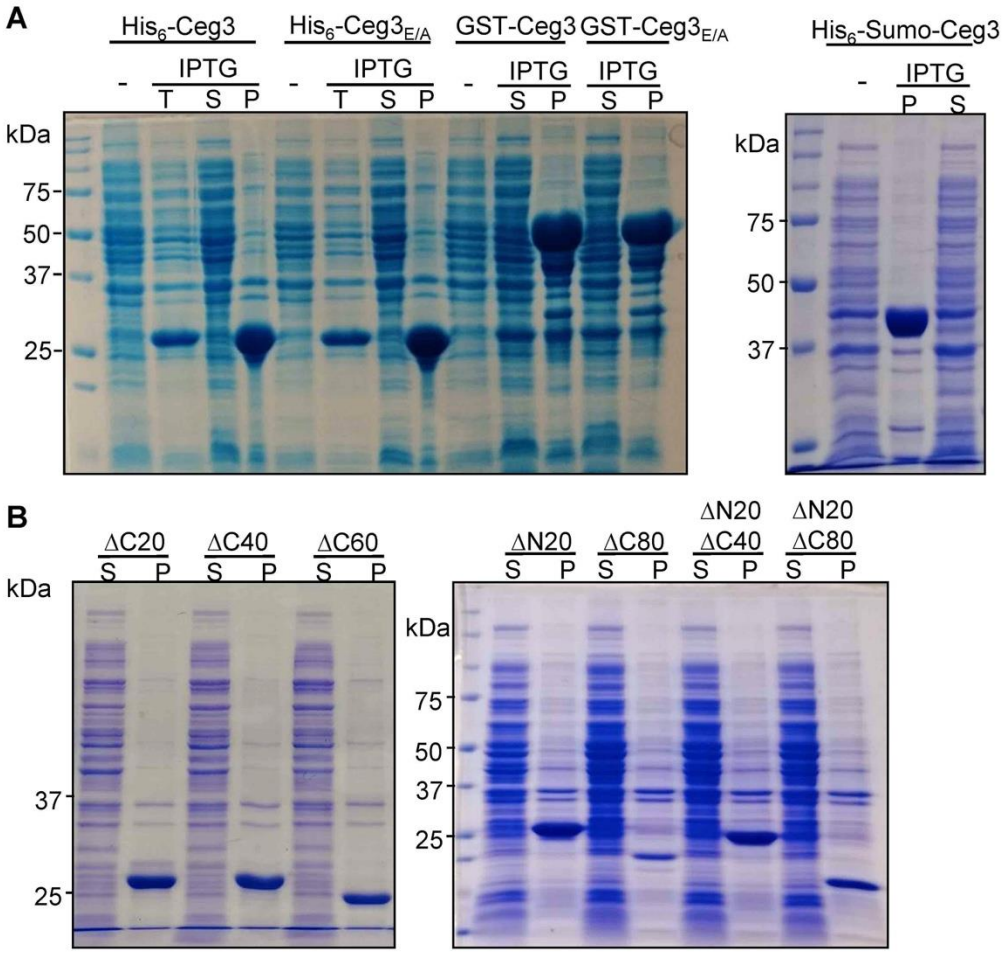

Fig. S3 Recombinant Ceg3 expressed in *E. coli* is insoluble

A. Solubility of His_6-, GST-, or His_6-Sumo-tagged Ceg3 in *E. coli*. *E. coli* strains harboring the appropriate plasmids were induced to express the differently tagged Ceg3 proteins with 0.2 mM IPTG. Soluble fractions obtained by centrifugation were resolved by SDS-PAGE and detected by Coomassie staining. -, no IPTG treatment; T, total lysates; S, supernatant fraction; P, pellet fraction.

B. Truncation mutagenesis did not yield a soluble version of Ceg3 in *E. coli*. Lysates of cells expressing His_6-tagged truncations were centrifugated to obtain soluble fractions and the presence of the proteins of interest was detected by Coomassie staining. S, supernatant fraction; P, pellet fraction.

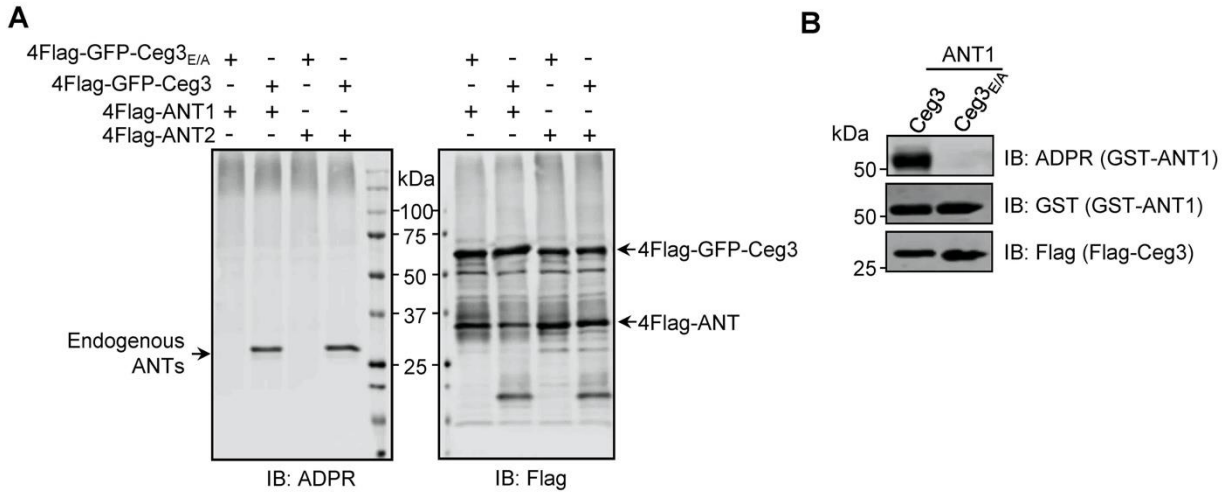

Fig. S4 ANT1 is ADP-ribosylated by Ceg3 in *E. coli*.

A. Proteins purified from mammalian cells do not detectably modify ADP/ATP translocases in a cell-free assay. 4xFlag-GFP-Ceg3 and 4xFlag-ANTs proteins purified from HEK293T cells were incubated with 1 mM NAD at 37°C for 1 h. Samples resolved by SDS-PAGE were probed for ADPR modification or for the relevant proteins. Note the detection of ADPR signals for modified endogenous ANTs.

B. *E. coli* strains harboring the appropriate plasmids were induced to express Flag-Ceg3 and GST-ANT1 proteins with 0.2 mM IPTG. Bacterial lysates resolved by SDS-PAGE were probed for ADPR modification and the expression of Flag-Ceg3 and GST-ANT1.

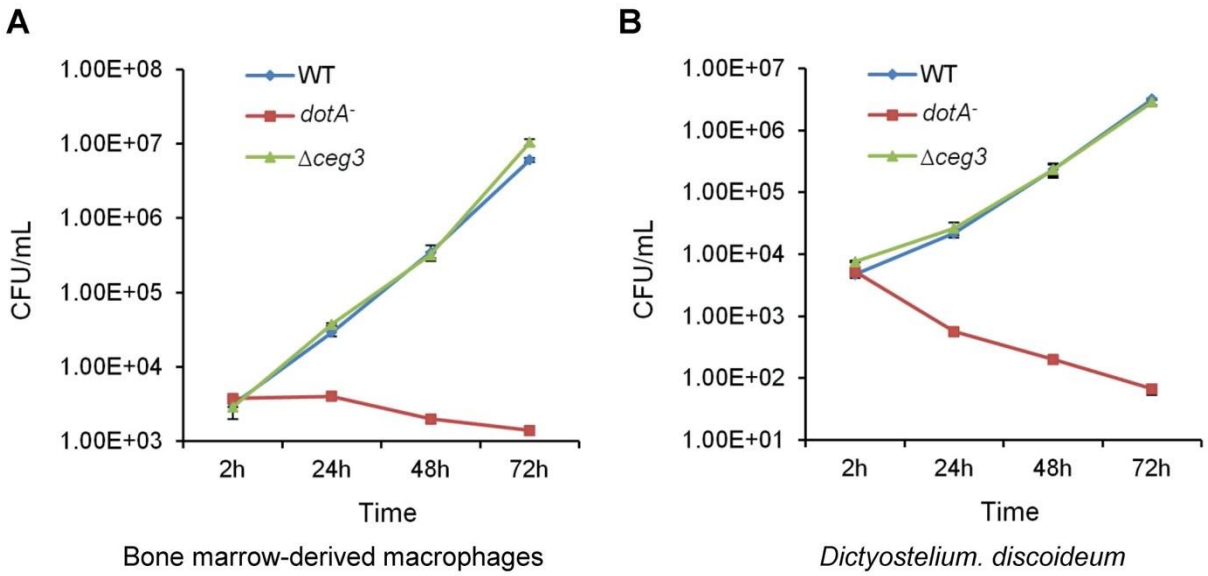

Fig. S5 Deletion of *ceg3* did not detectably affect intracellular growth of *L. pneumophila*. BMDMs (A) or *D. discoideum* (B) were infected with the indicated bacterial strains and intracellular bacteria were determined at the indicated time points. Each strain was done in triplicate and similar results were obtained in three independent experiments. Errors were derived from three technical replicates (mean ± s.e. from three replicates).

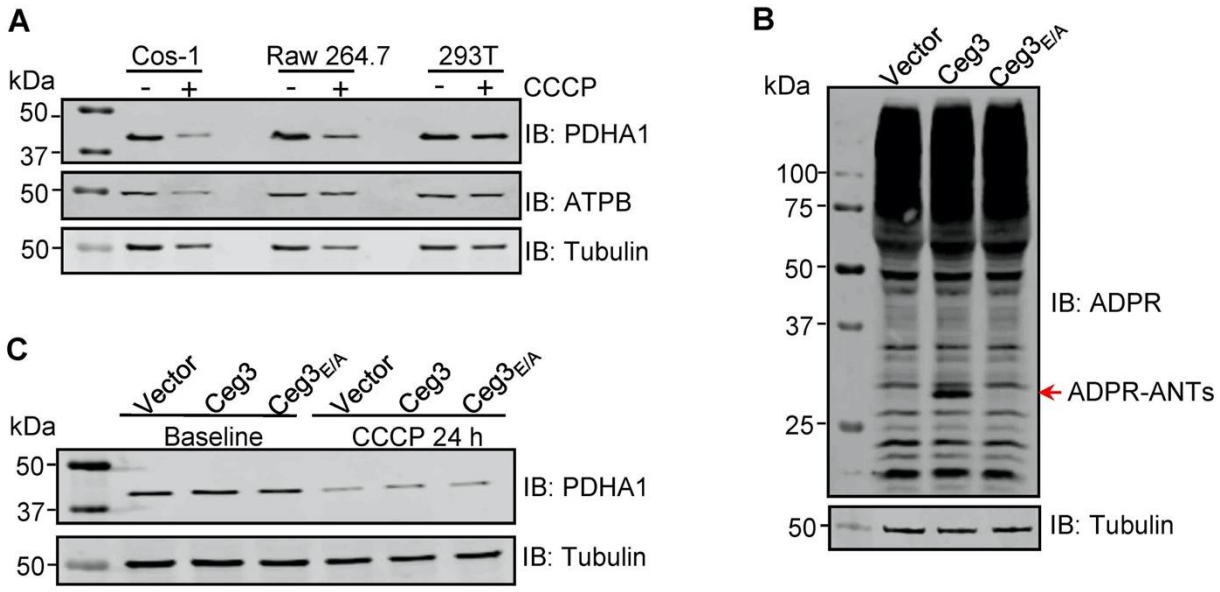

Fig. S6 ADP-ribosylation of ANTs by Ceg3 does not affect mitophagy induction

A. CCCP induces mitophagy in COS-1 cells. Lysates of the indicated cell lines that have been treated with 20 μM CCCP for 24 h were resolved by SDS-PAGE and then probed for PDHA1 (mitochondrial matrix protein) and ATPB (mitochondrial inner membrane protein). Tubulin was probed as a loading control.

B. Ceg3 expressed in COS-1 cells by lentiviral transduction induced ADP-ribosylation of ADP/ATP translocase. Lysates of COS-1 cells transduced with a lentivirus harboring the indicated plasmid at an MOI of 10 for two days were probed for ADPR modification, tubulin was probed as a loading control.

C. Ceg3 expressed in COS-1 cells does not affect the protein level of PDHA1 regardless of CCCP treatment. COS-1 cells expressing the indicated proteins for one day were treated with 20 μM CCCP for another 24 h, cells treated with DMSO were used as controls. PDHA1 was probed to evaluate mitophagy, tubulin was detected as a loading control.

TableS1 Identification of ADP/ATP translocases as the targets of Ceg3 in samples obtained by Af1521-pulldown. The protein band specifically present in Af1521 pulldown samples from expressing Ceg3 was analyzed by mass spectrometry; the 10 proteins with the most hits were listed.

Rank	Gene Name	Protein Description	Spectral Counts
1	KRT1	Keratin 1	232
2	SLC25A6	ADP/ATP translocase 3	87
3	SLC25A5	ADP/ATP translocase 2	84
4	SLC25A4	ADP/ATP translocase 1	71
5	KRT10	Keratin, type I cytoskeletal 10	64
6	KRT2	Keratin, type II cytoskeletal 2	57
7	KRT9	Keratin, type I cytoskeletal 9	56
8	SLC25A31	ADP/ATP translocase 4	40
9	KRT9	Keratin, type I cytoskeletal 9	36
10	KRT13	Keratin, type I cytoskeletal 13	29

1085 **Table S2 Bacterial strains, plasmids and primers used in this study**

Bacterial Strains	Source	Identifier
L. pneumophila (Philadelphia-1) LP02	(67)	N/A
L. pneumophila LP03	(67)	N/A
LP02Δ*ceg3*	This study	N/A
LP02Δ*ceg3* (pZL507)	This study	N/A
LP02Δ*ceg3* (pZLQ-Flag)	This study	N/A
LP02Δ*ceg3* (pCeg3)	This study	N/A
LP02Δ*ceg3* (pCeg3$_{E141A/E143A}$)	This study	N/A
LP02 (pCeg3)	This study	N/A
LP03 (pCeg3)	This study	N/A
E.coli BL21(DE3)	NEB	CAT#C2527I
E.coli XL1-Blue	Agilent	CAT#200249

1086

Plasmids	Source	Identifier
pZL507	(12)	N/A
pZLQ-Falg::*ceg3*	This study	N/A
pZLQ-Flag::*ceg3*$_{E141A/E143A}$	This study	N/A
p4xFlagCMV	(12)	N/A
p4xFlagCMV::*ceg3*	This study	N/A
p4xFlagCMV::*ceg3*$_{E141A/E143A}$	This study	N/A
pAPH-HA	This study	N/A
pAPH-HA::*ceg3*	This study	N/A
pAPH-HA::*ceg3*$_{E141A/E143A}$	This study	N/A
pCDNA3.1::*ceg3-Flag*	This study	N/A
GFP	(12)	N/A
GFP::*ceg3*	This study	N/A
GFP::*ceg3*$_{E141A/E143A}$	This study	N/A
pQE30	Qiagen	CAT#32915
pQE30::*ceg3*	This study	N/A
pQE30::*ceg3*$_{E141A/E143A}$	This study	N/A
pGST	Cytiva	CAT#28954648
pGST::*ceg3*	This study	N/A
pGST::*ceg3*$_{E141A/E143A}$	This study	N/A
pETSumo::*ceg3*	This study	N/A

pQE30::*ceg3ΔC20*	This study	N/A
pQE30::*ceg3ΔC40*	This study	N/A
pQE30::*ceg3ΔC60*	This study	N/A
pQE30::*ceg3ΔC80*	This study	N/A
pQE30::*ceg3ΔN20*	This study	N/A
pQE30::*ceg3ΔN20ΔC40*	This study	N/A
pQE30::*ceg3ΔN20ΔC80*	This study	N/A
p4xFlagCMV::*mavC*	(11)	N/A
p4xFlagCMV::*ANT1*	This study	N/A
p4xFlagCMV::$ANT1_{V227K/R237K}$	This study	N/A
p4xFlagCMV::*ANT2*	This study	N/A
p4xFlagCMV::*ANT3*	This study	N/A
p4xFlagCMV::*ANT4*	This study	N/A
pYES1NTA	Invitrogen	Cat#V825220
pYES1NTA::*ceg3*	This study	N/A
pYES1NTA::$ceg3_{E141A/E143A}$	This study	N/A
RFP::*ANT1*	This study	N/A
p4xFlagCMV::$ANT1_{R60K}$	This study	N/A
p4xFlagCMV::$ANT1_{R72K}$	This study	N/A
p4xFlagCMV::$ANT1_{R138K}$	This study	N/A
p4xFlagCMV::$ANT1_{R140K}$	This study	N/A
p4xFlagCMV::$ANT1_{R152K}$	This study	N/A
p4xFlagCMV::$ANT1_{R235K}$	This study	N/A
p4xFlagCMV::$ANT1_{R236K}$	This study	N/A
p4xFlagCMV::$ANT1_{R237K}$	This study	N/A
pCDH-CMV-MCS-EF1a-RFP	System Biosciences	Cat#CD512B-1
pCDH-CMV-MCS-EF1a-RFP:: *ceg3*	This study	N/A
pCDH-CMV-MCS-EF1a-RFP::$ceg3_{E141A/E143A}$	This study	N/A
pMD2.G	Addgene	Cat#12259
psPAX2	Addgene	Cat#12260

1087

Primers	**Sequence (Restriction enzyme sites are underlined)**	**Note**
pSL1001	ctaggatccatgaacagattaaaatttttttc	*ceg3* 5F BamHI
pSL1002	catgtcgacttaaactctaggggataatg	*ceg3* 3R SalI
pSL1003	catgtcgacgctggttattgcttggtgat	*ceg3* up SalI knockout
pSL1004	ctaggatccaagtaacgcattgtgaaatttg	*ceg3* up BamHI

		knockout
pSL1005	ctaggatccgttacttattatgtaaaggaatc	*ceg3* down BamHI
		knockout
pSL1006	catgagctcgcttaaagccactgcggttg	*ceg3* down SacI
		knockout
pSL1007	atcgacaaccagttctgcttttgccccgtcatgctcacc	*ceg3* $_{E141A/E143A}$ -1
pSL1008	ggtgagcatgacggggcaaaagcagaactggttgtcgat	*ceg3* $_{E141A/E143A}$ -2
pSL1009	ctagctagcgccaccatgaacagattaaaatttttttc	*ceg3* 5F NheI
pSL1010	catggatccttacttatcgtcgtcatccttgtaatcaactctaggggataatgaa	*ceg3* 3R BamHI
pSL1011	ctaggatccatgatttctaatttaagcgatcc	*ceg3*Δ*N20* 5F BamHI
pSL1012	catgtcgacttaatctccgtcaaatcgcctc	*ceg3*Δ*C20* 3R SalI
pSL1013	catgtcgacttaaagcttggcaaactcttc	*ceg3*Δ*C40* 3R SalI
pSL1014	catgtagacttacgaactgaaatcaccaagtt	*ceg3*Δ*C60* 3R SalI
pSL1015	catgtcgacttaattgggaaccactccccca	*ceg3*Δ*C80* 3R SalI
pSL1016	ctaggatccggtgatcacgcttggagct	*ANT1* 5F BamHI
pSL1017	catgtcgacttagacatatttttgatctcat	*ANT1* 3R SalI
pSL1018	ctatgatcaacagatgccgctgtgtcct	*ANT2* 5F BclI
pSL1019	catgtcgacttatgtgtacttcttgatttca	*ANT2* 3R SalI
pSL1020	ctaggatccacggaacaggccatctcct	*ANT3* 5F BamHI
pSL1021	catctcgagttagatcaccttcttgagctc	*ANT3* 3R XhoI
pSL1022	ctaggatcccatcgtgagcctgcgaaaaag	*ANT4* 5F BamHI
pSL1023	catgtcgacttacctaccaccaatatcaata	*ANT4* 3R SalI
pSL1024	cattgattgtgtggtgaaaatccctaaggagcagg	*ANT1*$_{R60K}$ -1
pSL1025	cctgctccttagggattttcaccacacaatcaatg	*ANT1*$_{R60K}$ -2
pSL1026	cttcctctccttctggaagggtaacctggc	*ANT1*$_{R72K}$ -1
pSL1027	gccaggttacccttccagaaggagaggaag	*ANT1*$_{R72K}$ -2
pSL1028	acccgctggactttgctaagaccaggttgg	*ANT1*$_{R138K}$ -1
pSL1029	ccaacctggtcttagcaaagtccagcgggt	*ANT1*$_{R138K}$ -2
pSL1030	gactttgctaggaccaagttggctgctgatgtg	*ANT1*$_{R140K}$ -1
pSL1031	cacatcagcagccaacttggtcctagcaaagtc	*ANT1*$_{R140K}$ -2
pSL1032	caagggcgccgcccagaaggagttccatggtctgg	*ANT1*$_{R152K}$ -1
pSL1033	ccagaccatggaactccttctgggcggcgcccttg	*ANT1*$_{R152K}$ -2
pSL1034	tcctacccctttgacactgttaagcgtagaatgatgatgcag	*ANT1*$_{R235K}$ -1
pSL1035	ctgcatcatcattctacgcttaacagtgtcaaaggggtagga	*ANT1*$_{R235K}$ -2
pSL1036	taccccttgacactgttcgtaagagaatgatgatgcagtc	*ANT1*$_{R236K}$ -1
pSL1037	gactgcatcatcattctcttacgaacagtgtcaaaggggta	*ANT1*$_{R236K}$ -2
pSL1038	tgacactgttcgtcgtaaaatgatgatgcagtccg	*ANT1*$_{R237K}$ -1

pSL1039	cggactgcatcatcattttacgacgaacagtgtca	*ANT1*$_{R237K}$-2
pSL1040	gcagtcgcagggctgaagtcctacccctttga	*ANT1*$_{V227K}$-1
pSL1041	tcaaaggggtaggacttcagccctgcgactgc	*ANT1*$_{V227K}$-2

1088

1089